Immunity

An Antigenic Atlas of HIV-1 Escape from Broadly Neutralizing Antibodies Distinguishes Functional and Structural Epitopes

Graphical Abstract
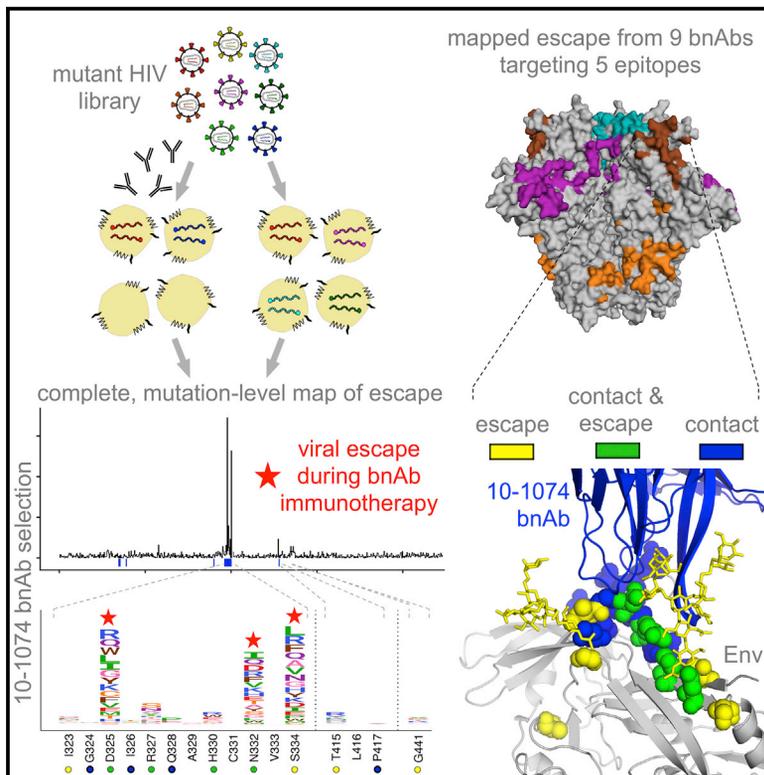
Authors

Adam S. Dingens, Dana Arenz, Haidyn Weight, Julie Overbaugh, Jesse D. Bloom

Correspondence

joverbau@fredhutch.org (J.O.), jbloom@fredhutch.org (J.D.B.)

In Brief

Dingens et al. mapped all possible single amino acid viral-escape mutations for a panel of HIV-1 broadly neutralizing antibodies that target major sites of vulnerability of HIV Env. This mutation-level antigenic atlas provides a comprehensive dataset for understanding viral immune escape and refining antibody-based immunotherapies and vaccines.

Highlights

- Mapped HIV Env escape from nine broadly neutralizing antibodies

- Functionally defined epitopes are distinct from structurally defined epitopes

- Maps of escape aid in interpreting viral mutations observed in immunotherapy trials

- The ease of escaping an antibody is related to but distinct from antibody breadth

CellPress

Immunity

Resource

CellPress

An Antigenic Atlas of HIV-1 Escape from Broadly Neutralizing Antibodies Distinguishes Functional and Structural Epitopes

Adam S. Dingens,[1,2,3] Dana Arenz,[3] Haidyn Weight,[3] Julie Overbaugh,[3,*] and Jesse D. Bloom[1,4,5,*]

[1]Basic Sciences Division and Computational Biology Program, Fred Hutchinson Cancer Research Center, Seattle, WA 98109, USA
[2]Molecular & Cellular Biology PhD Program, University of Washington, Seattle, WA 98195, USA
[3]Division of Human Biology and Epidemiology Program, Seattle, WA 98109, USA
[4]Howard Hughes Medical Institute, Seattle, WA 98109, USA
[5]Lead Contact
*Correspondence: joverbau@fredhutch.org (J.O.), jbloom@fredhutch.org (J.D.B.)
https://doi.org/10.1016/j.immuni.2018.12.017

SUMMARY

Anti-HIV broadly neutralizing antibodies (bnAbs) have revealed vaccine targets on the virus's envelope (Env) protein and are themselves promising immunotherapies. The efficacy of bnAb-based therapies and vaccines depends in part on how readily the virus can escape neutralization. Although structural studies can define contacts between bnAbs and Env, only functional studies can define mutations that confer escape. Here, we mapped how all possible single amino acid mutations in Env affect neutralization of HIV by nine bnAbs targeting five epitopes. For most bnAbs, mutations at only a small fraction of structurally defined contact sites mediated escape, and most escape occurred at sites near, but not in direct contact with, the antibody. The Env mutations selected by two pooled bnAbs were similar to those expected from the combination of the bnAbs's independent action. Overall, our mutation-level antigenic atlas provides a comprehensive dataset for understanding viral immune escape and refining therapies and vaccines.

INTRODUCTION

Over the last decade, a burgeoning number of broadly neutralizing antibodies (bnAbs) have been isolated from HIV-infected humans. These antibodies target conserved regions of the HIV envelope (Env) that are promising vaccine targets (Kwong and Mascola, 2018). Additionally, their broad neutralizing activity and potential to direct the killing of infected cells make bnAbs promising antiviral immunotherapeutic drugs for HIV prevention, therapy, and cure strategies (Margolis et al., 2017; Pegu et al., 2017).

However, bnAbs face a formidable foe. HIV Env's exceptional evolutionary capacity allows the virus to stay one step ahead of bnAbs during infection, and resistance often arises when bnAbs are therapeutically administered to infected animals (Klein et al.,

2012; Poignard et al., 1999; Shingai et al., 2013) or humans (Bar et al., 2016; Caskey et al., 2015, 2017; Lynch et al., 2015a; Scheid et al., 2016; Trkola et al., 2005). Thus, defining mutations that mediate viral escape is essential to optimizing and evaluating bnAb immunotherapies and vaccines.

Although extensive efforts have gone into structurally characterizing bnAb epitopes via X-ray crystallography and cryo-electron microscopy (cryo-EM), structures on their own are insufficient to completely define functional epitopes (Cunningham and Wells, 1993; Kelley and O'Connell, 1993), defined here as sites where mutations affect antibody neutralization of replication-competent viruses. Making individual mutations to Env and performing neutralization assays can provide information on the functional effect of specific mutations, but even the largest studies employing one-at-a-time mutagenesis can only assay a small fraction of all possible Env mutations.

We recently described mutational antigenic profiling, a massively parallel experimental approach to quantify how all single amino acid mutations to Env affect antibody neutralization (Dingens et al., 2017). This approach involves generating libraries of HIV that carry all Env amino acid mutations compatible with viral replication, incubating these libraries with or without an antibody, infecting T cells, and using deep sequencing to quantify the enrichment of each mutation in the selected versus nonselected libraries. Here, we applied this approach to a panel of nine bnAbs that target five Env epitopes, as well as to a pool of two bnAbs. The resulting maps of viral escape provide comprehensive mutation-level views of the functional interfaces between HIV and bnAbs.

RESULTS

Complete Maps of Viral Escape Define the Functional Epitopes for a Panel of bnAbs

To gain a broad picture of viral escape, we selected nine bnAbs targeting the five best-characterized epitopes on Env (Figure 1A). Specifically, the bnAb panel includes the CD4 binding site (CD4bs) bnAbs VRC01 (Wu et al., 2010) and 3BNC117 (Scheid et al., 2011), the V3/N332 glycan supersite bnAbs PGT121 (Walker et al., 2011) and 10-1074 (Mouquet et al., 2012), the V2 apex bnAbs PG9 (Walker et al., 2009) and PGT145 (Walker et al., 2011), the fusion peptide and gp120-gp41 interface bnAbs

CellPress
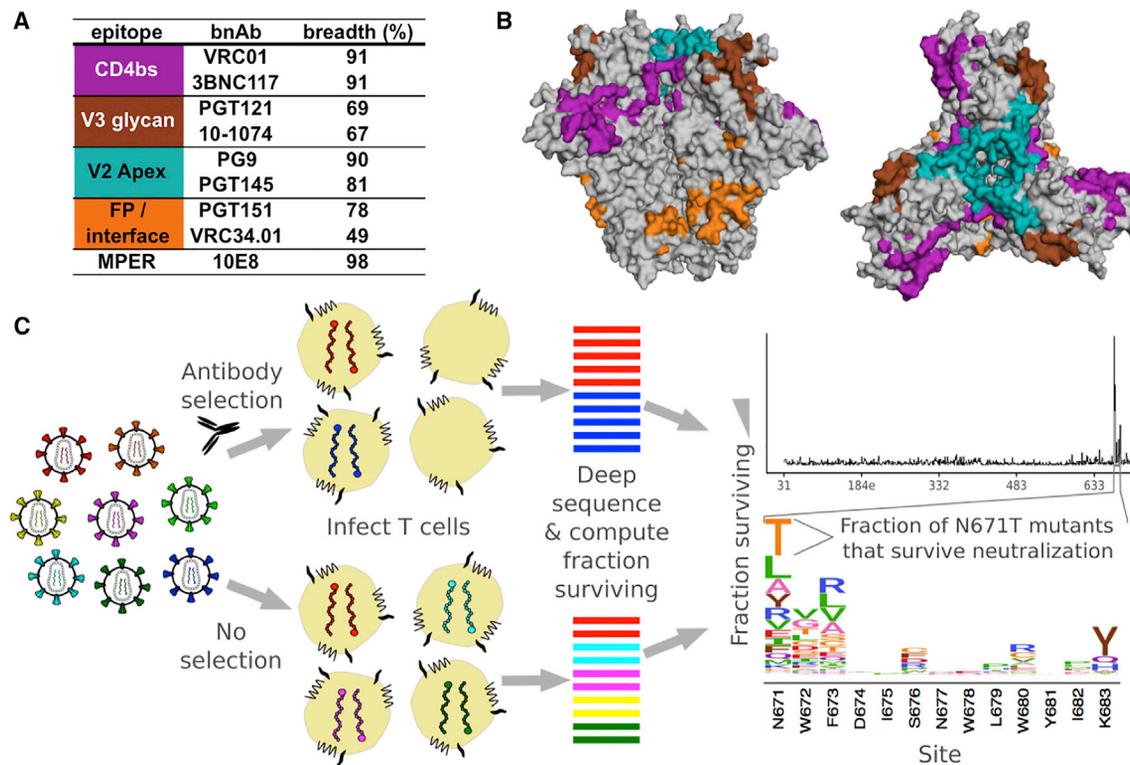
Figure 1. Schematic of Mutational Antigenic Profiling of a Panel of bnAbs

(A) The bnAb panel. Breadth measures are from the 100 most commonly used viruses on Los Alamos National Laboratory's CATNAP (Yoon et al., 2015).

(B) For each epitope, structurally defined antibody contact sites are indicated by colors on the side and top views of the BG505 SOSIP Env trimer (PDB: 5FYL).

(C) The mutational antigenic profiling experimental workflow and example data from bnAb 10E8. A mutant virus library is incubated with or without an antibody before infecting SupT1.CCR5 cells. Non-integrated viral cDNA from infected cells is deep sequenced to quantify the frequency of each *env* mutation in both the antibody-selected and mock-selected conditions, and the overall fraction of the virus library that survives antibody neutralization is quantified via qPCR. The fraction of each mutant that survives neutralization is plotted at the site level in line plots and at the mutation level in logoplots. The height of each letter is proportional to the fraction of the virions with that amino acid that survived antibody selection in excess of the overall library average.

PGT151 (Falkowska et al., 2014) and N123-VRC34.01 (subsequently referred to as VRC34.01; Kong et al., 2016), and the membrane-proximal external region (MPER) bnAb 10E8 (Huang et al., 2012). The binding footprints of these antibodies have been previously characterized using structural techniques (Figure 1B), allowing us to compare the structural epitopes with the functional epitopes defined by this study.

We mapped escape from these antibodies using the BG505.T332N Env, which is from a transmitted-founder subtype A HIV strain (Wu et al., 2006). This Env trimer is used widely in structural and vaccination studies (Sanders et al., 2013; Ward and Wilson, 2017). We used viral libraries that were previously generated by making all possible amino acid mutations to the ectodomain and transmembrane domain of Env. There are 19 amino acid mutations × 670 sites = 12,730 such amino acid mutations, and our libraries contain the subset of these mutations that is compatible with viral growth in cell culture (Haddox et al., 2018).

To quantify how each of these mutations affect HIV's antibody sensitivity, we neutralized independently generated mutant virus libraries at an ~IC95–IC99.9 antibody concentration and deep sequenced the *env* genes of viruses that were able to infect cells in the presence of the antibody (Figure 1C). For each antibody,

we performed at least two replicates using independently generated viral libraries (Figure S1). We performed parallel control experiments without the antibody and compared the relative frequency of each Env mutation in the antibody-selected library to that of the non-selected control. By scaling this relative frequency by the overall fraction of the entire library that survived the antibody selection, we estimated the fraction of virions with each mutation that survived the selection, hereafter termed the "fraction surviving" (Doud et al., 2018). To highlight escape mutations, we plotted the excess fraction surviving above the overall library average.

Each antibody reproducibly selected mutations at just a small subset of Env sites (Figures 2A and S1). The entire mutation-level maps of viral escape from each antibody are plotted across the entire mutagenized portion of *env* in Data S1. Antibodies targeting the same epitope tended to select mutations in similar regions of Env, and these mutations clustered in three-dimensional structures in or near the antibody-binding footprint (Figure 2A). This is exemplified by PG9 and PGT145, where the selected positions largely overlapped. Note also that the effect size of mutations varied across antibodies (compare the y axes in Figure 2A), as did the apparent noise in the plots; the implications of this are discussed in more detail in a later Results subsection.
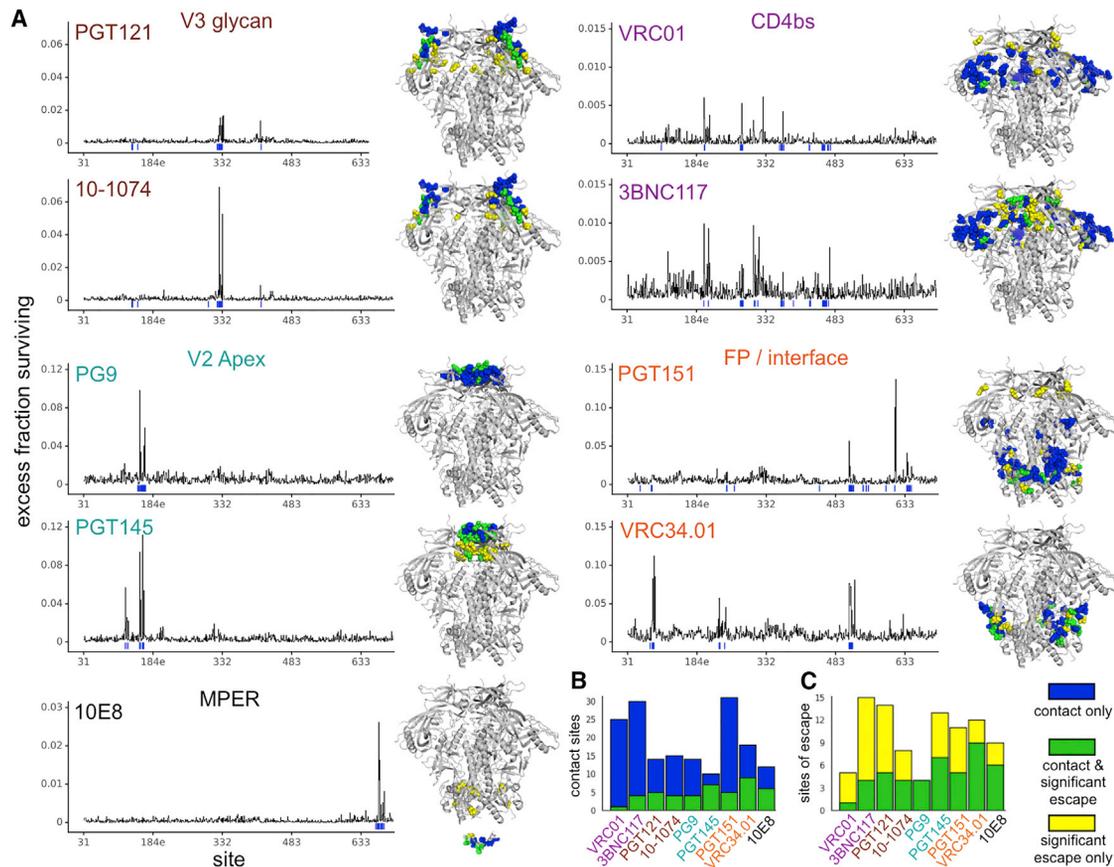
Figure 2. Env-wide Escape Profiles Distinguish Functional from Structural Antibody Epitopes

(A) The line plots show the excess fraction surviving antibody neutralization averaged across all mutations at each site. Structurally defined contact sites are indicated by a blue line. The structures show the BG505 Env SOSIP trimer (PDB: 5FYL) with sites of significant escape colored yellow, contact sites colored blue, and overlap between these sets of sites colored green. For 10E8, the MPER peptide structure (which is absent from the SOSIP trimer) is also shown (PDB: 4G6F).
(B) Bars give the number of structurally defined contact sites for each antibody, and green indicates the contact sites that are also sites of significant escape.
(C) Bars give the number of sites of significant escape for each antibody, and green indicates the sites of escape that are also contact sites. The green bars encompass the same sets of sites in (B) and (C). Median values across all biological replicates were plotted; see Figure S1 for the number of experimental replicates. See also Figures S2 and S3.

To rigorously compare the overlap between structural contacts and sites of viral escape, we identified sites of significant functional escape from the mutational antigenic profiling data and sites of physical contact between the bnAb and Env from published structures. We defined significant sites of viral escape by fitting a gamma distribution to the measured antigenic effects of mutations at each site and identified sites where the antigenic effects were larger than expected from this distribution at a false discovery rate of 0.01 (Figures S2A and S2B). We defined sites of structural contact as Env residues that were within 4 Å of the antibody in available structural models, only considering non-hydrogen atoms (see STAR Methods for details).

For most antibodies, only a small fraction of the structurally defined contact sites were also sites of significant viral escape (Figures 2B and S2C). Further, we identified numerous sites of escape outside the structurally defined epitope for most antibodies. The extent to which escape occurred at sites that directly contact the antibody differed considerably across bnAbs, ranging from all significant sites of escape for PG9 to only one of five sites of escape for VRC01 (Figures 2C and S2C). The sites of escape that do not directly contact the antibody are usually near the structurally defined epitope in the 5–10 Å range (Figure S2C). However, a few sites of escape were more distant from the structurally defined epitope (Figures 2A and S2D).

Although our maps of escape included most mutations previously identified using individual BG505 point-mutant pseudoviruses in TZM-bl neutralization assays (Kong et al., 2016; Lee et al., 2017), we also uncovered many previously uncharacterized sites of escape. We generated and tested BG505 point-mutant pseudoviruses in TZM-bl neutralization assays for three antibodies, testing 16–19 point mutants for each antibody. The measurements from the mutational antigenic profiling were well-correlated with the fold change in IC_{50} (inhibitory concentration 50) from TZM-bl neutralization assays for all antibodies tested (PGT121: R = 0.76, n = 16; 10-1074: R = 0.81, n = 16; VRC01: R = 0.69, n = 19) (Figure S3). In the next few subsections, we focus on each Env epitope individually.

Escape from V3-Glycan Supersite bnAbs Reveals Differences in Escape between Clonal Antibody Variants

The two anti-V3 antibodies PGT121 and 10-1074 are clonal variants that arose in the same infected individual (Mouquet et al., 2012). However, there were intriguing differences between the two antibodies in the specific mutations that mediated escape in our experiments, as well as between the overall effect sizes of escape mutations (Figures 3A and 3B, note the different y axis scales in the two panels). For instance, mutations at site 325 had a larger effect on 10-1074 than on PGT121, whereas mutations at site 327 had similar effects. We validated the differential effects of mutations to site 325 by testing three different mutants at this site in TZM-bl neutralization assays: the maximal effect for 10-1074 was a 27-fold increase in IC_{50}, whereas the maximal effect for PGT121 was just a 1.7-fold increase (D325E; Figure S3). Our mutational antigenic profiling also indicated that mutations that eliminated the N332 glycan had a larger effect for 10-1074 than for PGT121 (Figures 3A and 3B), which is consistent with a prior study that examined binding to gp120 (Mouquet et al., 2012). In contrast, at most other sites in the epitope (such as 323, 327, and 330), the overall effects of mutations were similar between the two antibodies (Figures 3A and 3B).

There are also differences in *which* mutations at a given site escape each antibody. For example, although the overall effect of all mutations at site 330 was similar for 10-1074 and PGT121, H330R escapes 10-1074 but not PGT121 (Figures 3A and 3B, validated by TZM-bl neutralization assays in Figure S3). Even among small-effect mutations, TZM-bl neutralization assays validated the results of mutational antigenic profiling. For example, mutations at site 325 had disparate effects: D325E had a large effect on 10-1074 but a negligible effect on PGT121, D325S had a small effect on 10-1074 but no effect on PGT121, and D325N had no effect on either antibody (Figures 3A and 3B, validated in Figure S3).

The basis for differences in the magnitude and specificity of escape between PGT121 and 10-1074 may be explained by their differential somatic hypermutation. There are numerous differences in the portions of these two antibodies that contact the N332 glycan (Figure S4), and these differences have previously been shown to affect glycan recognition (Mouquet et al., 2012). In contrast, antibody residues that directly contact site 325 are conserved between PGT121 and 10-1074 (Figure S4). However, there are numerous differences in the light-chain variable loops near these contact sites that may be responsible for the differential effects of mutations at site 325 on the two antibodies.

Many aspects of our maps of escape were consistent with prior knowledge about the epitopes of these two antibodies (Garces et al., 2014; Mouquet et al., 2012; Sok et al., 2014, 2016). For example, eliminating the targeted N332 glycan via mutations to N332 and S334 resulted in escape from both antibodies, as did antibody-specific mutations in the [324]GDIR[327] motif (Figure 3), a conserved region of this epitope that is involved with CCR5 co-receptor binding (Sok et al., 2016).

However, we also identified escape at sites not previously implicated as being part of the functional epitope. For instance, viral escape from both antibodies occurred via mutations at site 415 in V4 and to a modest but reproducible extent at site 441 (Figures 3A and 3B). We validated that mutations at each of these sites resulted in escape from both antibodies in TZM-bl neutralization assays (Figure S3). Neither of these sites directly interact with either antibody; site 415 is close to other structural contacts, as well as to the N332 glycan, and site 441 in the β22 strand neighbors the N301 glycan.

Escape from V2 Apex bnAbs Can Occur via Altering Charges in and Near the Trimer Interface

For the V2-apex antibodies PG9 and PGT145, escape occurred via elimination of the N160 glycan at the heart of the epitope (Figures 2A, 3D, and 3E). Additionally, escape occurred at structurally defined contact sites at the trimer apex for PG9 and at the trimer apex and interface for PGT145. For both antibodies, prior studies suggest that binding is driven by electrostatic interactions with positively charged Env residues (Lee et al., 2017; McLellan et al., 2011; Wang et al., 2017). Mutations to these sites resulted in viral escape (including residues R166, K169, and K171 for PG9 and K121, R161, and K169 for PGT145), with charge swaps often resulting in the greatest extent of escape (Figures 3D and 3E). Structural studies indicate that the long HCDR3 (heavy chain complementarity-determining region 3) arm of PGT145 reaches into the trimer interface; existence of this epitope has been hypothesized to result from a balancing act of a "push" from inter-protomer charge repulsions at the trimer interface and a "pull" of hydrophobic interactions between variable loops across protomers at the trimer apex (Lee et al., 2017).

While escape from PGT145 occurred by eliminating the epitope's positive charges, escape also occurred by *introducing* charges at sites where the wild-type residue is not charged. These included sites 123, 124, and 127 in or very near the epitope, as well as more distant sites encircling the epitope, including sites 200, 202, and 203 in the β3–β4 loop and 312, 313, and 315 at the tip of the V3 loop (Figure 3F). These mutations presumably also affected the charge repulsions at the trimer interface and/or overall trimer conformation, disrupting the electrostatic balancing act that is crucial for PGT145 binding.

Escape from CD4bs bnAbs Reveals Distinct Interprotomer Dynamics in Escape

Escape from CD4bs bnAbs VRC01 and 3BNC117 occurred in both the canonically defined CD4bs epitope and other sites distal to the CD4 binding site (Figures 2A and 4). In the CD4 binding site, mutations to site 279 in loop D and site 369 in the CD4 binding loop escaped both antibodies (Figure 4A). With the exception of sites 279 and 280, the specific amino acid mutations in loop D that mediated escape differed between VRC01 and 3BNC117.

The largest-effect mutations for both antibodies introduced a serine or threonine in place of the asparagine at site 197. The N197 glycan is part of a glycan fence that shields the CD4bs (Crooks et al., 2017). N197S and N197T (N197S/T) both eliminate this N197 glycan and introduce a new potential N-linked glycosylation motif (PNG) at N195. Because escape was only mediated by S/T at site 197, these data suggest that eliminating N197 alone does not result in viral escape, but shifting the N197 glycan to N195 does. We validated these observations using point mutants in TZM-bl neutralization assays: simply
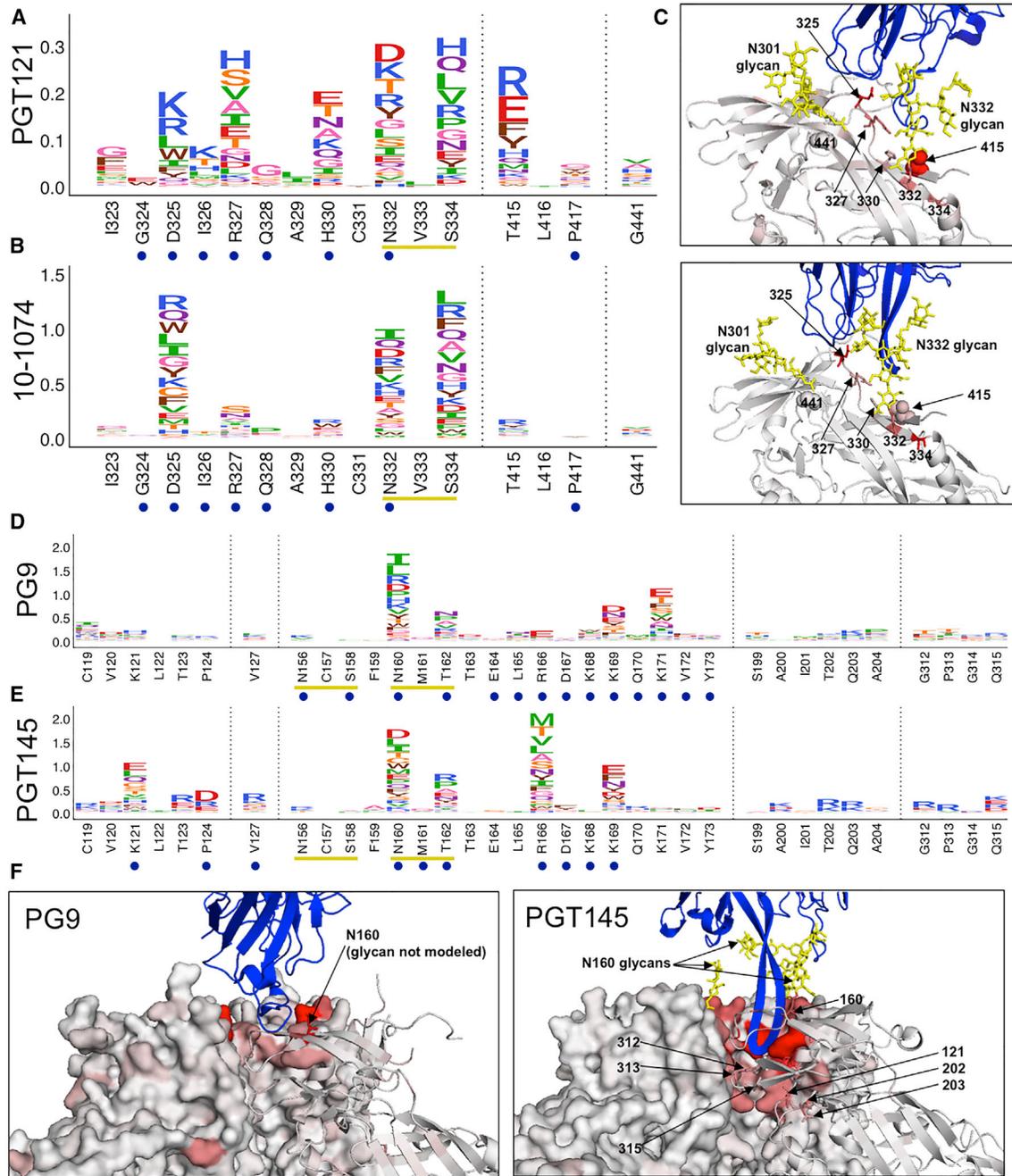
Figure 3. Escape from V3-Glycan Supersite and V2 Apex bnAbs

(A and B) Escape profiles for V3-glycan supersite bnAbs PGT121 (A) and 10-1074 (B). Letter heights indicate the excess fraction surviving for each mutation. Blue circles indicate structurally defined contact sites, and yellow underlines indicate a N-linked glycosylation motif. Logoplots that show escape across Env are in Data S1.

(C) V3-glycan supersite antibodies are shown in blue, and Env is colored according to the maximum excess fraction surviving at each site. Note that for PGT121, the closely related clonal variant PGT122 structure is used in lieu of a PGT121 structure (PDB: 5FYL and 5T3Z, respectively).

(D and E) Escape profiles of V2 apex antibodies PG9 (D) and PGT145 (E) presented in the same manner as (A) and (B).

(F) V2 apex antibodies are shown in blue, and Env is colored according to the maximum excess fraction surviving at each site (PDB: 5VJ6 and 5V8L, respectively). Median values across all biological replicates were plotted; see Figure S1 for the number of experimental replicates. See also Figures S2 and S3.
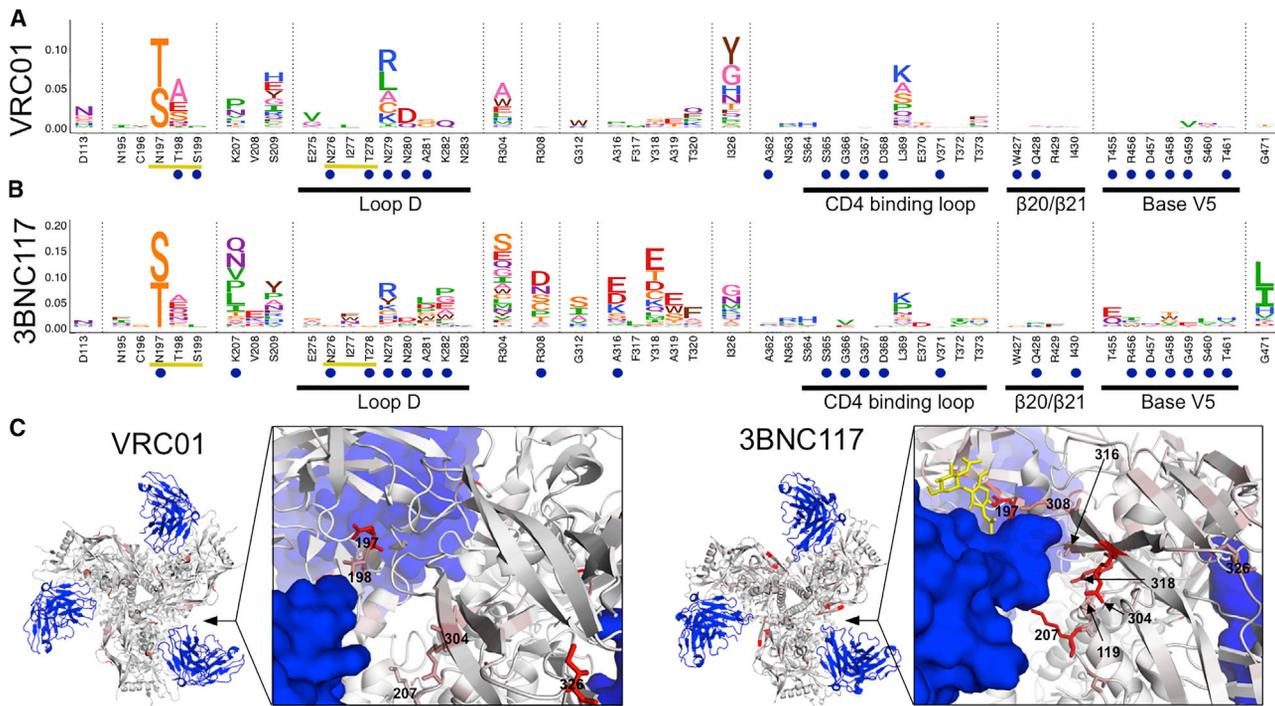
Figure 4. Escape from CD4bs bnAbs

(A and B) Escape profiles for CD4bs bnAbs VRC01 (A) and 3BNC117 (B). Letter heights indicate the excess fraction surviving for each mutation. Blue circles indicate structurally defined contact sites, and yellow underlines indicate a N-linked glycosylation motif. Portions of the canonical CD4bs epitope are underlined in black and labeled. Logoplots that show escape across Env are in Data S1.

(C) Antibodies are shown in blue, and Env is colored according to the average fraction surviving at each site (PDB: 5FYK and 5V8M, respectively). Median values across all biological replicates were plotted; see Figure S1 for the number of experimental replicates. See also Figures S2 and S3.

eliminating the N197 PNG via N197E resulted in ~50-fold more potent neutralization by VRC01, whereas N197S resulted in viral escape, increasing the IC$_{50}$ by 27-fold relative to wild-type (Figure S3).

Escape from both antibodies also occurred via D113N, which introduces a PNG at site 113. Site 113 is in the trimer interface distant from the CD4bs (Figure 4C), suggesting that this mutation may affect exposure of the CD4bs epitope by altering trimer conformation or dynamics. We validated that D113N resulted in escape from VRC01 by using a TZM-bl neutralization assay (Figure S3). Although it is unknown if the PNG created by D113N is indeed glycosylated, these data show that altering potential glycosylation sites both near and distal to the epitope can affect CD4bs bnAb neutralization.

Escape from 3BNC117 also occurred at numerous sites near where the antibody's HCDR3 arm makes inter-protomer contacts, including sites in V3 (sites 304, 308, 312, and 316–320) and at the base of the β3–β4 loop (sites 207 and 209) (Figure 4B). This quaternary nature of the 3BNC117 epitope was first postulated based on early trimer structures (Lyumkis et al., 2013), and higher resolution cryo-EM of the BG505 trimer in complex with 3BNC117 (Lee et al., 2017) confirmed that 3BNC117 directly interacts with residues 207, 308, and 316 from the neighboring protomer (Figures 4B and 4C). It has been previously reported that mutations to site 207 result in decreased 3BNC117 binding (Liu et al., 2017). We also observed viral escape from 3BNC117

at site I326, a site distal to 3BNC117 near the base of the V3 loop that takes part in variable-loop hydrophobic interactions that may regulate trimer dynamics (Lee et al., 2017).

Although VRC01 does not make inter-protomer structural contacts similar to those of 3BNC117 (Stewart-Jones et al., 2016), we still observed escape at sites 207, 209, 304, and 326 (Figures 4A and 4C). We validated that I326Y results in escape from VRC01 (Figure S3) but has little effect on the V3-specific bnAbs 10-1074 and PGT121, despite these antibodies directly contacting this site.

Escape from Fusion Peptide and gp120-gp41 Interface bnAbs Differs Despite Similarities in Structurally Defined Contacts

Maps of escape from PGT151 and VRC34.01 highlight the complex nature of the conformational fusion peptide and gp120-gp41 interface epitope (Figures 2A, 5A, and 5B). Here, we reanalyzed VRC34.01 mutational antigenic profiling data from a prior study (Dingens et al., 2018), quantifying the effects of mutations using the fraction surviving metric rather than the differential selection metric used in the earlier study, and compared these data to the BG505 Env escape from PGT151 reported here. Although both antibodies contact the 6 N-terminal residues of the fusion peptide (512–517), escape from PGT151 is focused on just the 3 N-terminal residues of this peptide (512–514), whereas escape from VRC34.01 is mediated by numerous
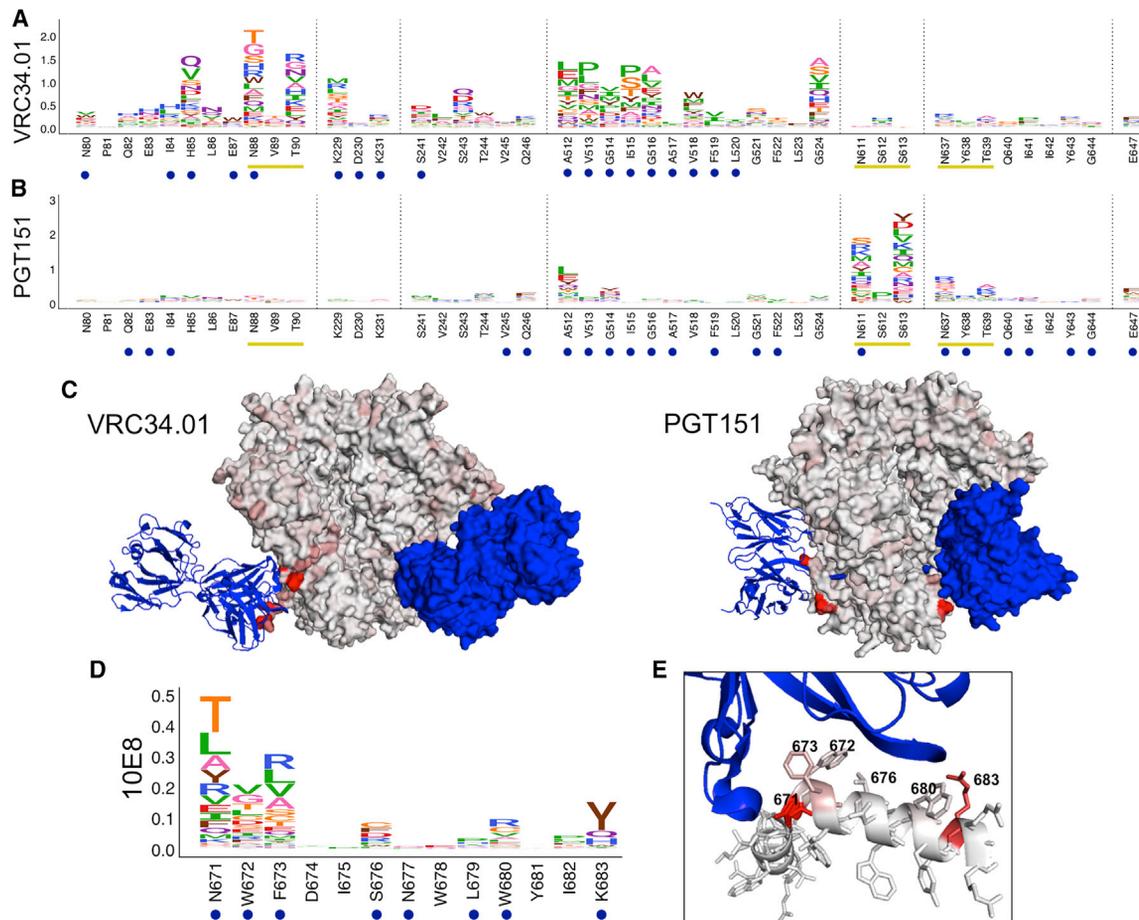
Figure 5. Escape from Fusion Peptide-Interface and MPER bnAbs

(A and B) Escape profiles for fusion peptide and gp120-gp41 interface bnAbs VRC34.01 (A) and PGT151 (B). Letter heights indicate the excess fraction surviving for each mutation. Logoplots that show escape across Env are in Data S1.

(C) Fusion peptide antibodies are shown in blue, and Env is colored according to the maximum excess fraction surviving at each site (PDB: 5I8H and 5FUU, respectively).

(D) Escape profile for MPER bnAb 10E8 presented in the same manner as in (A) and (B).

(E) 10E8 is shown in blue, and the MPER peptide is colored according to the maximum excess fraction surviving at each site (PDB: 4G6F). Median values across all biological replicates were plotted; see Figure S1 for the number of experimental replicates. See also Figures S2 and S3.

mutations to sites 512–516 and 518. The structural footprints of both antibodies center on the fusion peptide, but they contact distinct glycans and protein regions of gp120 and gp41. Again, their functional epitopes included distinct subsets of these protein residues and glycans (Figures 5A and 5B). For both antibodies, there were also numerous sites of significant escape at non-contact sites near the epitope (Figures 5A and 5B). For PGT151, we also identified sites of escape at more distant residues in V3; the mechanisms of escape at these sites are unclear.

Escape from an MPER bnAB

Escape from the MPER-directed antibody 10E8 occurred predominantly in the structurally defined contact sites, and sites of escape were localized to one side of the MPER peptide α helix apical to 10E8 (Figures 5D and 5E) (Huang et al., 2012). This agrees precisely with prior studies (Huang et al., 2012; Kim et al., 2014). However, we identified two additional modest, but significant, sites of escape outside of the MPER peptide, at sites

609 and 643 in the C-C loop and HR2 domain of gp41, respectively (Figures 2A and S2B). Mutations at these sites may alter fusion kinetics and/or the presentation of the MPER epitope.

Maps of Escape Identify Sites of *In Vivo* Escape during bnAb Immunotherapies in Humans

Several of the bnAbs that we characterized have been used in human immunotherapy studies. Some of the escape mutations identified in our work overlap with mutations that arose in the humans during these studies (Table S1). For example, when 10-1074 was administered to HIV-infected individuals, viral escape mutations emerged at site 325 and at the PNG that encompasses sites 332 and 334 (Caskey et al., 2017). These are the same three sites where the strongest selection is observed in our 10-1074 mutational antigenic profiling (Figure 3B; Table S1).

There was also considerable overlap between sites of escape we mapped *in vitro* and those that occurred *in vivo* during treatment of infected individuals with the CD4bs antibodies 3BNC117

CellPress
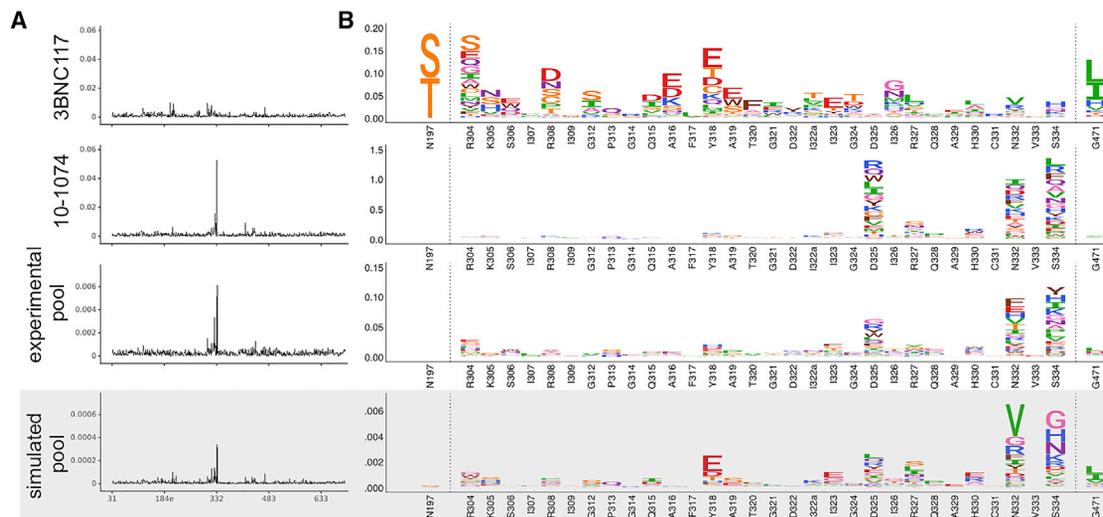
Figure 6. Escape from 3BNC117 and 10-1074 Pooled bnAbs

(A) The excess fraction surviving neutralization averaged across all mutations at each site. Data from Figure 3 (10-1074) and Figure 4 (3BNC117) are re-plotted for relevant sites. For the pooled 3BNC117 and 10-1074 data, the mean value across six replicates is plotted. The simulated data are the product of each antibody's mean excess mutation fraction surviving values.

(B) A logoplot zooming in on epitope regions for each dataset.

In (A) and (B), the simulated data is distinguished from the experimental data with a light gray overlay. See also Figure S1.

or VRC01. For 3BNC117, the sites that overlap between our maps and human trials (Caskey et al., 2015; Schoofs et al., 2016) included sites 182, 209, 279, 308, 318, and 471 (Table S1). Site 279 is one of the strongest sites of escape from 3BNC117 and VRC01 in our experiments. A mutation to site 279 is part of the viral escape pathway within the patient from whom VRC01 was isolated (Lynch et al., 2015b) and arose during VRC01 immunotherapy post treatment interruption (Bar et al., 2016). Mutations to site 279 also played a role in escaping a CD4bs-targeted response in another patient (Wibmer et al., 2013) and during 3BNC117 immunotherapy of infected individuals (Caskey et al., 2015; Schoofs et al., 2016).

Our data may also be useful for identifying previously unappreciated escape mutations during immunotherapy. For example, after patient V10 underwent therapy with VRC01 (Bar et al., 2016) a rare amino acid variant at site 326 was fixed in the viral population (Table S1), but the potential significance of this mutation was not noted in the original publication because it is far from the structural epitope. Our mutational antigenic profiling revealed that mutations at site 326 increase resistance to VRC01 (Figure 4A), demonstrating how comprehensive maps of mutational escape can aid in interpreting clinical data.

Escape from Pooled Antibodies Is Similar to the Modeled Combination of Their Independent Actions

Many immunotherapy studies are beginning to treat patients with combinations of bnAbs. For instance, a recently completed set of clinical trials involved treating patients with equal concentrations of 3BNC117 and 10-1074 (Bar-On et al., 2018; Mendoza et al., 2018). We therefore investigated how escape from a mix of these two antibodies compares to escape from each antibody individually.

We pooled the antibodies at equal concentrations, then selected our viral libraries with the antibody pool (Figures 6 and S1). Escape from the pooled antibodies appeared to be a combination of the escape profiles from each antibody in isolation (Figures 6A and 6B). For example, we observed escape at sites 325, 332, and 334, likely associated with escape from 10-1074, as well as escape at sites 304, 308, and 471, which presumably affect 3BNC117 resistance.

Escape from the pooled antibodies does not occur at sites where the escape mutation from one antibody sensitizes the virus to the other. For instance, the strongest escape mutations for 3BNC117 alone are N197S and N197T, which shift the N197 glycan to N195 (Figures 4B and 6A). However, eliminating the N197 glycan increased the virus's susceptibility to neutralization by antibodies targeting the same epitope as 10-1074 (Liang et al., 2016; Townsley et al., 2015). Mutations at site N197 were not selected by the pool of antibodies in our mutational antigenic profiling, presumably because any benefit with respect to escaping 3BNC117 is canceled out by increased susceptibility to 10-1074. This example demonstrates the potential for suppressing viral escape mutations by selecting antibodies with synergistic effects at specific sites.

To model the synergistic effects of antibodies on suppressing viral escape, we calculated the expected escape profile from a pool of 10-1074 and 3BNC117 by simply taking the product of each mutation's excess fraction-surviving value for each antibody (Figure 6). The rationale behind this calculation was that the expected fraction of virions with a mutation that should survive both antibodies is simply the product of the fraction that would survive each antibody individually. The escape profile predicted by this simple model closely matched the actual selection from the pooled antibodies (Figure 6).
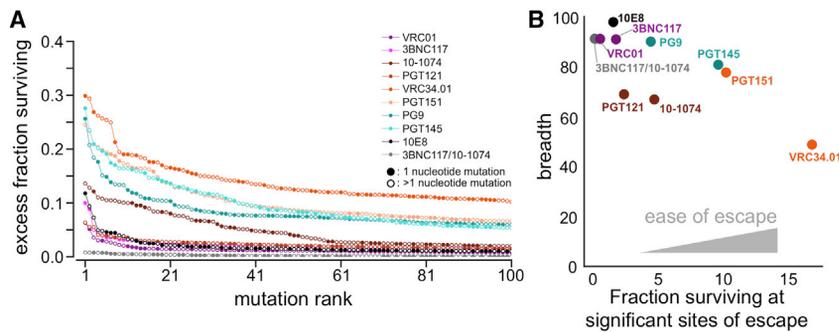
Figure 7. Quantifying the Ability to Escape Each bnAb

(A) The excess fraction surviving for the 100 largest-effect mutations for each antibody. Closed circles indicate mutations that are one nucleotide mutation away from BG505 wild-type, whereas open circles indicate mutations that are 2 or 3 nucleotide mutations away from BG505 wild-type sequence.

(B) Each antibody's breadth (as quantified in Figure 1) is plotted against the sum of the excess mutation fraction-surviving values at all significant sites of viral escape.

Overall, these data suggested that no single amino acid mutations robustly escape both 3BNC117 and 10-1074. Rather, the low-level escape from the pooled antibodies appeared to represent mutations that escape one antibody but have little effect on the other. Furthermore, the similarity of the experimentally measured escape profile for the pooled antibodies and the profile predicted from the product of the individual antibody profiles suggested that our maps of escape from single antibodies could be useful for computationally predicting the potential for escape from antibody pools.

The Ability of the BG505 Env to Escape Each bnAb with Single Mutations Is Related to but Distinct from Antibody Breadth

Anti-HIV bnAbs are often evaluated in terms of their breadth and potency against panels of naturally occurring viral strains. Our data offer the opportunity to calculate an alternative measure relevant to the potential efficacy of bnAb immunotherapies: the ability of single amino acid mutations to increase the antibody resistance of a particular viral strain.

We used our mutational antigenic profiling to assess the ease of single-mutation escape of the BG505 Env from each antibody. First, we simply qualitatively examined the 100 largest effect-size mutations for each antibody (Figure 7A). For some antibodies (such as VRC34.01), there are many individual mutations that efficiently escape neutralization—but for other antibodies (such as VRC01), only a few mutations affect escape and do so with only moderate size effects (Figure 7A). For all of the antibodies, at least some of the largest effect-size mutations were accessible by single-nucleotide mutations, indicating that the genetic code only has moderate effects on the accessibility of escape mutations (Figure 7A).

To quantify the ease with which the BG505 Env can escape each antibody by single mutations, we summed the excess mutation fraction-surviving values at each significant site of viral escape. This single-mutation ease-of-escape metric was moderately correlated with the antibody's breadth (Figure 7B). But, especially for the broadest antibodies, there were differences between neutralization breadth on natural strains and ease of single amino acid escape by BG505 (Figure 7B). For example, 10E8 had 98% breadth and VRC01 had 91% breadth, but BG505 had more capacity to escape 10E8 by single amino acid mutations. Differences in the extent of natural sequence variation at epitopes potentially contributes to the differences between breadth and the ease of escape; many of the escape

mutations we identify are rarely observed in nature (Foley et al., 2017) (Figure S5). These results highlighted that, similar to influenza antibodies (Doud et al., 2018), HIV bnAb breadth on natural strains and the potential for single-mutation escape by any given viral variant are distinct measures, both of which may be useful for assessing the potential for viral antibody escape in clinical settings.

Mapping Differences in Escape across Diverse Envs Quantifies Strain-Specific Differences in Viral Escape

All of the foregoing results are for Env from a single viral strain, BG505. Although it is well known that the effect of mutations on antibody neutralization can differ from strain to strain, there are no unbiased quantifications of how much the antigenic effects of mutations typically shift across strains. To address this question, we also mapped escape from VRC01 and PGT151 using LAI Env, a subtype B strain (Figures S1, S6, and S7; Data S2). In addition, we compared our maps of escape from PGT151 in BG505 and LAI to our previously published map of escape from this antibody by the subtype A BF520 Env (Dingens et al., 2017).

Escape from PGT151 across all three strains is quite similar. The dominant escape mutations are in the N611 and N637 PNGs, as well as in sites in the fusion peptide and the HR-2 domain (Figure S6; Data S2). However, there are a number of sites where single mutations mediated escape in LAI but not in BG505 or BF520 (sites 82, 84, 224, 229, 242, 245, 521, 602, and 603). Many of the escape mutations unique to LAI are clustered near the epitope, suggesting that LAI may adopt a different local conformation (Figure S6B). We validated three of these strain-specific escape mutations using TZM-bl neutralization assays and found that the strain differences in both antigenic effects and mutational tolerance appear to play a role in shaping these differences (Figure S6D).

There were relatively more strain-specific differences in escape from VRC01 than from PGT151 (Figure S7; Data S2). Mutations to site 279 escaped VRC01 in both Envs but with larger effects in LAI (Figure S7B). N197S/T escaped VRC01 in BG505 but not in LAI. There is a clear mechanistic basis for this difference: N197S/T shifts the N197 PNG to N195 in BG505, whereas N197S/T only disrupts the N197 PNG in LAI. In contrast, D113N introduces a glycan in both strains but only escaped VRC01 in BG505 (Figure S7B, validated in TZM-bl assays in Figure S7D). Further, I326Y and L369K escaped VRC01 in BG505 but not in LAI (also validated in TZM-bl assays in Figure S7D), whereas

mutations to site 474 generally have a larger effect in LAI than in BG505 (Figure S7B).

A possible explanation for the differences in VRC01 escape is differences in Env conformational dynamics. BG505 is generally well behaved as a SOSIP trimer, adopting a prefusion "closed" state (Verkerke et al., 2016), whereas LAI is a lab-adapted strain that likely adopts a more "open" conformation (Munro et al., 2014). We speculate that the mutations outside of the CD4bs, such D113N or I326Y, could disrupt BG505's trimer structure or dynamics resulting in escape from VRC01, but the same mutations to LAI may not disrupt a "closed" state if it is less frequently or not adopted by LAI.

DISCUSSION

We have mapped how all single amino acid mutations to the BG505 Env affect neutralization of replication-competent HIV by nine prototypical bnAbs. These maps of viral escape define the functional epitopes of these antibodies, which we show are distinct from the structurally defined epitopes. For all antibodies, viral escape occurred at only a fraction of structurally defined contact sites, and many escape mutations occurred at sites outside the direct structurally defined epitope. This escape at non-contact sites often clustered close to the structural contacts, suggesting that altering a network of interacting sites near the structural epitope can disrupt antibody binding or neutralization. In a few cases, escape also occurred at sites more distant from the epitope, likely due to alterations in the conformation or dynamics of Env.

Others have previously noted that not all structurally defined contact sites affect antibody binding (Falkowska et al., 2012; Kelley and O'Connell, 1993; Li et al., 2011), and mutations outside of the structural epitope can affect antibody sensitivity (Back et al., 1993; Blish et al., 2008; Boyd et al., 2015; Bradley et al., 2016; O'Rourke et al., 2012; Sethi et al., 2013). However, our complete maps of escape mutations make it possible to systematically quantify the overlap between the functional and structural epitopes of bnAbs. Our work also highlights how incompletely prior structural and virological assays have defined the functionally relevant interactions between HIV and antibodies. Even though our study focused on some of the best-characterized anti-HIV bnAbs, we uncovered numerous sites in Env (often outside of the structural epitope) where mutations were not previously known to affect bnAb sensitivity.

One application for which our maps of viral escape may be of immediate use is evaluating bnAb immunotherapies. During immunotherapy trials, many viral mutations arise, and it is important to know which ones alter sensitivity to the bnAb used in the trial (Bar et al., 2016; Caskey et al., 2015, 2017; Lynch et al., 2015a; Scheid et al., 2016; Schoofs et al., 2016). Although our maps, of course, do not perfectly predict escape that occurs *in vivo*, which could be influenced by many stochastic factors, including the specific variant that infected the individual, they do define functional epitopes that can be used to help assess the potential antigenic significance of viral mutations. For instance, our map of the functional epitope of VRC01 allowed us to re-interpret the potential significance of a previously unremarked-upon mutation

outside the structural epitope that occurred during VRC01 immunotherapy.

We also examined how our maps of escape from individual antibodies compared to those generated using a pool of antibodies—an important question, because combinations of bnAbs are a clear future direction in antibody immunotherapy (Wagh et al., 2016, 2018). We mapped escape from a pool of two bnAbs, 3BNC117 and 10-1074, and we found that there were no mutations that robustly escaped both antibodies. This finding agrees with the results of two recently completed clinical trials that administered this antibody combination and did not report selection of any mutations that conferred resistance to both antibodies (Bar-On et al., 2018; Mendoza et al., 2018). Further, the combined selection of the two antibodies was similar to that predicted from the product of the individual escape profiles. Therefore, antigenic maps for individual antibodies may be useful for modeling viral escape from combinations of antibodies.

Our data also provide a way to quantify the ease with which the BG505 Env can escape from each antibody via single mutations. Although this ease-of-escape metric contains many caveats specific to our experimental system (it considered only single mutations to BG505 that support viral replication in cell culture, omitting the effect of insertions and deletions), caveats also apply to other methods for estimating how likely a virus is to escape an antibody. For example, characterizing viral escape during immunotherapy in animal models often examines only a single viral strain in a limited number of animals. We found that BG505's ease of escape by single mutations is correlated with antibody breadth against natural sequences, but that there are also differences, especially among the broadest antibodies. We suggest that both measures may be useful for assessing the potential efficacy of bnAb-based therapies.

Of course, it is important to keep in mind that our maps only measure the effect of single amino acid mutations to BG505. Epistatic interactions among multiple mutations can play a role in viral fitness and immune evasion (Adams et al., 2017; Dahirel et al., 2011; Lynch et al., 2015b; Otsuka et al., 2018; da Silva et al., 2010; Troyer et al., 2009; Wu et al., 2017). Additionally, we performed most of our experiments in the single genetic background of the BG505 Env, but the effects of mutations on viral growth and antigenicity sometimes differ among viral strains (Barton et al., 2016; Falkowska et al., 2014; Haddox et al., 2018). However, we did compare maps of escape from a few antibodies across viral strains. Escape from PGT151 was quite similar across strains, whereas escape from VRC01 was more variable between strains. Further studies contrasting escape from additional antibodies across additional strains are needed to better define strain-specific effects in antibody escape.

Nonetheless, having complete antigenic maps of the BG505 Env versus a panel of important bnAbs provides a wealth of information that can help guide the study of HIV evolution and the development of anti-viral strategies. Future work that combines these antigenic maps with measurements (Haddox et al., 2016, 2018) or models (Louie et al., 2018; Shekhar et al., 2013; Zanini et al., 2017) of how mutations affect HIV's replicative fitness could shed further light on the virus's evolutionary dynamics under immune pressure.

CellPress

STAR★METHODS

Detailed methods are provided in the online version of this paper and include the following:

- KEY RESOURCES TABLE
- CONTACT FOR REAGENT AND RESOURCE SHARING
- EXPERIMENTAL MODEL AND SUBJECT DETAILS
- METHOD DETAILS
  - Generation of Mutant Virus Libraries
  - Mutational Antigenic Profiling
  - Barcoded Subamplicon Deep Sequencing
  - Structural Analyses
  - TZM-bl Neutralization Assays
- QUANTIFICATION AND STATISTICAL ANALYSIS
  - Analysis of Deep Sequencing Data and Computation of Fraction Surviving
  - Identification of Significant Sites of Viral Escape
- DATA AND SOFTWARE AVAILABILITY

SUPPLEMENTAL INFORMATION

Supplemental Information includes seven figures, one table, and four data files and can be found with this article online at https://doi.org/10.1016/j.immuni.2018.12.017.

AUTHOR CONTRIBUTIONS

Conceptualization, A.S.D.; Methodology, A.S.D., and J.D.B.; Validation, A.S.D., D.A., and H.W.; Investigation, A.S.D.; Software, A.S.D. and J.D.B.; Supervision, J.O. and J.D.B.; Writing – Original Draft, A.S.D.; Writing – Review & Editing, A.S.D., J.O., and J.D.B.; Funding Acquisition, J.O. and J.D.B.

DECLARATION OF INTERESTS

The authors declare no competing interests.

REFERENCES

Adams, R.M., Kinney, J.B., Walczak, A.M., and Mora, T. (2017). Physical epistatic landscape of antibody binding affinity. arXiv, arXiv:1712.04000, https://arxiv.org/abs/1712.04000.

Back, N.K., Smit, L., Schutten, M., Nara, P.L., Tersmette, M., and Goudsmit, J. (1993). Mutations in human immunodeficiency virus type 1 gp41 affect sensitivity to neutralization by gp120 antibodies. J. Virol. 67, 6897–6902.

Bar, K.J., Sneller, M.C., Harrison, L.J., Justement, J.S., Overton, E.T., Petrone, M.E., Salantes, D.B., Seamon, C.A., Scheinfeld, B., Kwan, R.W., et al. (2016). Effect of HIV Antibody VRC01 on Viral Rebound after Treatment Interruption. N. Engl. J. Med. 375, 2037–2050.

Bar-On, Y., Gruell, H., Schoofs, T., Pai, J.A., Nogueira, L., Butler, A.L., Millard, K., Lehmann, C., Suárez, I., Oliveira, T.Y., et al. (2018). Safety and antiviral activity of combination HIV-1 broadly neutralizing antibodies in viremic individuals. Nat. Med. 24, 1701–1707.

Barton, J.P., Goonetilleke, N., Butler, T.C., Walker, B.D., McMichael, A.J., and Chakraborty, A.K. (2016). Relative rate and location of intra-host HIV evolution to evade cellular immunity are predictable. Nat. Commun. 7, 11660.

Benki, S., McClelland, R.S., Emery, S., Baeten, J.M., Richardson, B.A., Lavreys, L., Mandaliya, K., and Overbaugh, J. (2006). Quantification of genital human immunodeficiency virus type 1 (HIV-1) DNA in specimens from women with low plasma HIV-1 RNA levels typical of HIV-1 nontransmitters. J. Clin. Microbiol. 44, 4357–4362.

Blish, C.A., Nguyen, M.A., and Overbaugh, J. (2008). Enhancing exposure of HIV-1 neutralization epitopes through mutations in gp41. PLoS Med. 5, e9.

Bloom, J.D. (2015). Software for the analysis and visualization of deep mutational scanning data. BMC Bioinformatics 16, 168.

Boyd, D.F., Peterson, D., Haggarty, B.S., Jordan, A.P.O., Hogan, M.J., Goo, L., Hoxie, J.A., and Overbaugh, J. (2015). Mutations in HIV-1 envelope that enhance entry with the macaque CD4 receptor alter antibody recognition by disrupting quaternary interactions within the trimer. J. Virol. 89, 894–907.

Bradley, T., Trama, A., Tumba, N., Gray, E., Lu, X., Madani, N., Jahanbakhsh, F., Eaton, A., Xia, S.-M., Parks, R., et al. (2016). Amino Acid Changes in the HIV-1 gp41 Membrane Proximal Region Control Virus Neutralization Sensitivity. EBioMedicine 12, 196–207.

Caskey, M., Klein, F., Lorenzi, J.C.C., Seaman, M.S., West, A.P., Jr., Buckley, N., Kremer, G., Nogueira, L., Braunschweig, M., Scheid, J.F., et al. (2015). Viraemia suppressed in HIV-1-infected humans by broadly neutralizing antibody 3BNC117. Nature 522, 487–491.

Caskey, M., Schoofs, T., Gruell, H., Settler, A., Karagounis, T., Kreider, E.F., Murrell, B., Pfeifer, N., Nogueira, L., Oliveira, T.Y., et al. (2017). Antibody 10-1074 suppresses viremia in HIV-1-infected individuals. Nat. Med. 23, 185–191.

Crooks, G.E., Hon, G., Chandonia, J.-M., and Brenner, S.E. (2004). WebLogo: a sequence logo generator. Genome Res. 14, 1188–1190.

Crooks, E.T., Osawa, K., Tong, T., Grimley, S.L., Dai, Y.D., Whalen, R.G., Kulp, D.W., Menis, S., Schief, W.R., and Binley, J.M. (2017). Effects of partially dismantling the CD4 binding site glycan fence of HIV-1 Envelope glycoprotein trimers on neutralizing antibody induction. Virology 505, 193–209.

Cunningham, B.C., and Wells, J.A. (1993). Comparison of a structural and a functional epitope. J. Mol. Biol. 234, 554–563.

da Silva, J., Coetzer, M., Nedellec, R., Pastore, C., and Mosier, D.E. (2010). Fitness epistasis and constraints on adaptation in a human immunodeficiency virus type 1 protein region. Genetics 185, 293–303.

Dahirel, V., Shekhar, K., Pereyra, F., Miura, T., Artyomov, M., Talsania, S., Allen, T.M., Altfeld, M., Carrington, M., Irvine, D.J., et al. (2011). Coordinate linkage of HIV evolution reveals regions of immunological vulnerability. Proc. Natl. Acad. Sci. USA 108, 11530–11535.

Dingens, A.S., Haddox, H.K., Overbaugh, J., and Bloom, J.D. (2017). Comprehensive Mapping of HIV-1 Escape from a Broadly Neutralizing Antibody. Cell Host Microbe 21, 777–787.e4.

Dingens, A.S., Acharya, P., Haddox, H.K., Rawi, R., Xu, K., Chuang, G.-Y., Wei, H., Zhang, B., Mascola, J.R., Carragher, B., et al. (2018). Complete functional mapping of infection- and vaccine-elicited antibodies against the fusion peptide of HIV. PLoS Pathog. 14, e1007159.

Doud, M.B., Lee, J.M., and Bloom, J.D. (2018). How single mutations affect viral escape from broad and narrow antibodies to H1 influenza hemagglutinin. Nat. Commun. 9, 1386.

Falkowska, E., Ramos, A., Feng, Y., Zhou, T., Moquin, S., Walker, L.M., Wu, X., Seaman, M.S., Wrin, T., Kwong, P.D., et al. (2012). PGV04, an HIV-1 gp120 CD4 binding site antibody, is broad and potent in neutralization but does not induce conformational changes characteristic of CD4. J. Virol. *86*, 4394–4403.

Falkowska, E., Le, K.M., Ramos, A., Doores, K.J., Lee, J.H., Blattner, C., Ramirez, A., Derking, R., van Gils, M.J., Liang, C.-H., et al. (2014). Broadly neutralizing HIV antibodies define a glycan-dependent epitope on the prefusion conformation of gp41 on cleaved envelope trimers. Immunity *40*, 657–668.

Foley, B., Leitner, T., Apetrei, C., Hahn, B., Mizrachi, I., Mullins, J., Rambaut, A., Wolinsky, S., and Korber, B. (2017). HIV Sequence Compendium 2017. Theor. Biol. Biophys. Group, Los Alamos Natl. Lab. NM *LA-UR 17-2*. https://www.hiv.lanl.gov/content/sequence/HIV/COMPENDIUM/2017/sequence2017.pdf

Garces, F., Sok, D., Kong, L., McBride, R., Kim, H.J., Saye-Francisco, K.F., Julien, J.P., Hua, Y., Cupo, A., Moore, J.P., et al. (2014). Structural evolution of glycan recognition by a family of potent HIV antibodies. Cell *159*, 69–79.

Gristick, H.B., von Boehmer, L., West, A.P., Jr., Schamber, M., Gazumyan, A., Golijanin, J., Seaman, M.S., Fätkenheuer, G., Klein, F., Nussenzweig, M.C., et al. (2016). Natively glycosylated HIV-1 Env structure reveals new mode for antibody recognition of the CD4-binding site. Nat. Struct. Mol. Biol. *23*, 906–915.

Haddox, H.K., Dingens, A.S., and Bloom, J.D. (2016). Experimental Estimation of the Effects of All Amino-Acid Mutations to HIV's Envelope Protein on Viral Replication in Cell Culture. PLoS Pathog. *12*, e1006114.

Haddox, H.K., Dingens, A.S., Hilton, S.K., Overbaugh, J., and Bloom, J.D. (2018). Mapping mutational effects along the evolutionary landscape of HIV envelope. eLife *7*, e34420.

Huang, J., Ofek, G., Laub, L., Louder, M.K., Doria-Rose, N.A., Longo, N.S., Imamichi, H., Bailer, R.T., Chakrabarti, B., Sharma, S.K., et al. (2012). Broad and potent neutralization of HIV-1 by a gp41-specific human antibody. Nature *491*, 406–412.

Kelley, R.F., and O'Connell, M.P. (1993). Thermodynamic analysis of an antibody functional epitope. Biochemistry *32*, 6828–6835.

Kim, A.S., Leaman, D.P., and Zwick, M.B. (2014). Antibody to gp41 MPER alters functional properties of HIV-1 Env without complete neutralization. PLoS Pathog. *10*, e1004271.

Klein, F., Halper-Stromberg, A., Horwitz, J.A., Gruell, H., Scheid, J.F., Bournazos, S., Mouquet, H., Spatz, L.A., Diskin, R., Abadir, A., et al. (2012). HIV therapy by a combination of broadly neutralizing antibodies in humanized mice. Nature *492*, 118–122.

Kong, R., Xu, K., Zhou, T., Acharya, P., Lemmin, T., Liu, K., Ozorowski, G., Soto, C., Taft, J.D., Bailer, R.T., et al. (2016). Fusion peptide of HIV-1 as a site of vulnerability to neutralizing antibody. Science *352*, 828–833.

Kwong, P.D., and Mascola, J.R. (2018). HIV-1 Vaccines Based on Antibody Identification, B Cell Ontogeny, and Epitope Structure. Immunity *48*, 855–871.

Lee, J.H., Ozorowski, G., and Ward, A.B. (2016). Cryo-EM structure of a native, fully glycosylated, cleaved HIV-1 envelope trimer. Science *351*, 1043–1048.

Lee, J.H., Andrabi, R., Su, C.Y., Yasmeen, A., Julien, J.P., Kong, L., Wu, N.C., McBride, R., Sok, D., Pauthner, M., et al. (2017). A Broadly Neutralizing Antibody Targets the Dynamic HIV Envelope Trimer Apex via a Long, Rigidified, and Anionic β-Hairpin Structure. Immunity *46*, 690–702.

Li, Y., O'Dell, S., Walker, L.M., Wu, X., Guenaga, J., Feng, Y., Schmidt, S.D., McKee, K., Louder, M.K., Ledgerwood, J.E., et al. (2011). Mechanism of neutralization by the broadly neutralizing HIV-1 monoclonal antibody VRC01. J. Virol. *85*, 8954–8967.

Liang, Y., Guttman, M., Williams, J. a., Verkerke, H., Alvarado, D., Hu, S.-L., and Lee, K.K. (2016). Changes in structure and antigenicity of HIV-1 Env trimers resulting from removal of a conserved CD4 binding site-proximal glycan. J. Virol. *90*, 9224–9236.

Liu, Q., Acharya, P., Dolan, M.A., Zhang, P., Guzzo, C., Lu, J., Kwon, A., Gururani, D., Miao, H., Bylund, T., et al. (2017). Quaternary contact in the initial interaction of CD4 with the HIV-1 envelope trimer. Nat. Struct. Mol. Biol. *24*, 370–378.

Louie, R.H.Y., Kaczorowski, K.J., Barton, J.P., Chakraborty, A.K., and McKay, M.R. (2018). Fitness landscape of the human immunodeficiency virus envelope protein that is targeted by antibodies. Proc. Natl. Acad. Sci. USA *115*, E564–E573.

Lynch, R.M., Boritz, E., Coates, E.E., DeZure, A., Madden, P., Costner, P., Enama, M.E., Plummer, S., Holman, L., Hendel, C.S., et al. (2015a). Virologic effects of broadly neutralizing antibody VRC01 administration during chronic HIV-1 infection. Sci. Transl. Med. *7*, 319ra206.

Lynch, R.M., Wong, P., Tran, L., O'Dell, S., Nason, M.C., Li, Y., Wu, X., and Mascola, J.R. (2015b). HIV-1 fitness cost associated with escape from the VRC01 class of CD4 binding site neutralizing antibodies. J. Virol. *89*, 4201–4213.

Lyumkis, D., Julien, J.-P., de Val, N., Cupo, A., Potter, C.S., Klasse, P.-J., Burton, D.R., Sanders, R.W., Moore, J.P., Carragher, B., et al. (2013). Cryo-EM Structure of a Fully Glycosylated Soluble Cleaved HIV-1 Envelope Trimer. Science *342*, 1484–1490.

Margolis, D.M., Koup, R.A., and Ferrari, G. (2017). HIV antibodies for treatment of HIV infection. Immunol. Rev. *275*, 313–323.

McLellan, J.S., Pancera, M., Carrico, C., Gorman, J., Julien, J.-P., Khayat, R., Louder, R., Pejchal, R., Sastry, M., Dai, K., et al. (2011). Structure of HIV-1 gp120 V1/V2 domain with broadly neutralizing antibody PG9. Nature *480*, 336–343.

Mendoza, P., Gruell, H., Nogueira, L., Pai, J.A., Butler, A.L., Millard, K., Lehmann, C., Suárez, I., Oliveira, T.Y., Lorenzi, J.C.C., et al. (2018). Combination therapy with anti-HIV-1 antibodies maintains viral suppression. Nature *561*, 479–484.

Mouquet, H., Scharf, L., Euler, Z., Liu, Y., Eden, C., Scheid, J.F., Halper-Stromberg, A., Gnanapragasam, P.N.P., Spencer, D.I.R., Seaman, M.S., et al. (2012). Complex-type N-glycan recognition by potent broadly neutralizing HIV antibodies. Proc. Natl. Acad. Sci. USA *109*, E3268–E3277.

Munro, J.B., Gorman, J., Ma, X., Zhou, Z., Arthos, J., Burton, D.R., Koff, W.C., Courter, J.R., Smith, A.B., Kwong, P.D., et al. (2014). Conformational dynamics of single HIV-1 envelope trimers on the surface of native virions. Science *346*, 759–763.

O'Rourke, S.M., Schweighardt, B., Phung, P., Mesa, K.A., Vollrath, A.L., Tatsuno, G.P., To, B., Sinangil, F., Limoli, K., Wrin, T., and Berman, P.W. (2012). Sequences in glycoprotein gp41, the CD4 binding site, and the V2 domain regulate sensitivity and resistance of HIV-1 to broadly neutralizing antibodies. J. Virol. *86*, 12105–12114.

Otsuka, Y., Schmitt, K., Quinlan, B.D., Gardner, M.R., Alfant, B., Reich, A., Farzan, M., and Choe, H. (2018). Diverse pathways of escape from all well-characterized VRC01-class broadly neutralizing HIV-1 antibodies. PLoS Pathog. *14*, e1007238.

Pegu, A., Hessell, A.J., Mascola, J.R., and Haigwood, N.L. (2017). Use of broadly neutralizing antibodies for HIV-1 prevention. Immunol. Rev. *275*, 296–312.

Poignard, P., Sabbe, R., Picchio, G.R., Wang, M., Gulizia, R.J., Katinger, H., Parren, P.W.H.I., Mosier, D.E., and Burton, D.R. (1999). Neutralizing antibodies have limited effects on the control of established HIV-1 infection in vivo. Immunity *10*, 431–438.

Poss, M., and Overbaugh, J. (1999). Variants from the diverse virus population identified at seroconversion of a clade A human immunodeficiency virus type 1-infected woman have distinct biological properties. J. Virol. *73*, 5255–5264.

Sanders, R.W., Derking, R., Cupo, A., Julien, J.P., Yasmeen, A., de Val, N., Kim, H.J., Blattner, C., de la Peña, A.T., Korzun, J., et al. (2013). A next-generation cleaved, soluble HIV-1 Env trimer, BG505 SOSIP.664 gp140, expresses multiple epitopes for broadly neutralizing but not non-neutralizing antibodies. PLoS Pathog. *9*, e1003618.

Scheid, J.F., Mouquet, H., Ueberheide, B., Diskin, R., Klein, F., Oliveira, T.Y.K., Pietzsch, J., Fenyo, D., Abadir, A., Velinzon, K., et al. (2011). Sequence and structural convergence of broad and potent HIV antibodies that mimic CD4 binding. Science *333*, 1633–1637.

Scheid, J.F., Horwitz, J.A., Bar-On, Y., Kreider, E.F., Lu, C.-L., Lorenzi, J.C.C., Feldmann, A., Braunschweig, M., Nogueira, L., Oliveira, T., et al. (2016). HIV-1

CellPress

antibody 3BNC117 suppresses viral rebound in humans during treatment interruption. Nature 535, 556–560.

Schoofs, T., Klein, F., Braunschweig, M., Kreider, E.F., Feldmann, A., Nogueira, L., Oliveira, T., Lorenzi, J.C.C., Parrish, E.H., Learn, G.H., et al. (2016). HIV-1 therapy with monoclonal antibody 3BNC117 elicits host immune responses against HIV-1. Science 352, 997–1001.

Sethi, A., Tian, J., Derdeyn, C.A., Korber, B., and Gnanakaran, S. (2013). A mechanistic understanding of allosteric immune escape pathways in the HIV-1 envelope glycoprotein. PLoS Comput. Biol. 9, e1003046.

Shekhar, K., Ruberman, C.F., Ferguson, A.L., Barton, J.P., Kardar, M., and Chakraborty, A.K. (2013). Spin models inferred from patient-derived viral sequence data faithfully describe HIV fitness landscapes. Phys. Rev. E Stat. Nonlin. Soft Matter Phys. 88, 062705.

Shingai, M., Nishimura, Y., Klein, F., Mouquet, H., Donau, O.K., Plishka, R., Buckler-White, A., Seaman, M., Piatak, M., Jr., Lifson, J.D., et al. (2013). Antibody-mediated immunotherapy of macaques chronically infected with SHIV suppresses viraemia. Nature 503, 277–280.

Sok, D., Doores, K.J., Briney, B., Le, K.M., Saye-Francisco, K.L., Ramos, A., Kulp, D.W., Julien, J.-P., Menis, S., Wickramasinghe, L., et al. (2014). Promiscuous glycan site recognition by antibodies to the high-mannose patch of gp120 broadens neutralization of HIV. Sci. Transl. Med. 6, 236ra63.

Sok, D., Pauthner, M., Briney, B., Lee, J.H., Saye-Francisco, K.L., Hsueh, J., Ramos, A., Le, K.M., Jones, M., Jardine, J.G., et al. (2016). A Prominent Site of Antibody Vulnerability on HIV Envelope Incorporates a Motif Associated with CCR5 Binding and Its Camouflaging Glycans. Immunity 45, 31–45.

Stewart-Jones, G.B.E., Soto, C., Lemmin, T., Chuang, G.Y., Druz, A., Kong, R., Thomas, P.V., Wagh, K., Zhou, T., Behrens, A.J., et al. (2016). Trimeric HIV-1-Env Structures Define Glycan Shields from Clades A, B, and G. Cell 165, 813–826.

Townsley, S., Li, Y., Kozyrev, Y., Cleveland, B., and Hu, S.-L. (2015). Conserved Role of an N-Linked Glycan on the Surface Antigen of Human Immunodeficiency Virus Type 1 Modulating Virus Sensitivity to Broadly Neutralizing Antibodies against the Receptor and Coreceptor Binding Sites. J. Virol. 90, 829–841.

Trkola, A., Kuster, H., Rusert, P., Joos, B., Fischer, M., Leemann, C., Manrique, A., Huber, M., Rehr, M., Oxenius, A., et al. (2005). Delay of HIV-1 rebound after cessation of antiretroviral therapy through passive transfer of human neutralizing antibodies. Nat. Med. 11, 615–622.

Troyer, R.M., McNevin, J., Liu, Y., Zhang, S.C., Krizan, R.W., Abraha, A., Tebit, D.M., Zhao, H., Avila, S., Lobritz, M.A., et al. (2009). Variable fitness impact of HIV-1 escape mutations to cytotoxic T lymphocyte (CTL) response. PLoS Pathog. 5, e1000365.

Verkerke, H.P., Williams, J. a., Guttman, M., Simonich, C. a., Liang, Y., Filipavicius, M., Hu, S.-L., Overbaugh, J., and Lee, K.K. (2016). Epitope-independent purification of native-like envelope trimers from diverse HIV-1 isolates. J. Virol. 90, 9471–9482.

Wagh, K., Bhattacharya, T., Williamson, C., Robles, A., Bayne, M., Garrity, J., Rist, M., Rademeyer, C., Yoon, H., Lapedes, A., et al. (2016). Optimal Combinations of Broadly Neutralizing Antibodies for Prevention and Treatment of HIV-1 Clade C Infection. PLoS Pathog. 12, e1005520.

Wagh, K., Seaman, M.S., Zingg, M., Fitzsimons, T., Barouch, D.H., Burton, D.R., Connors, M., Ho, D.D., Mascola, J.R., Nussenzweig, M.C., et al. (2018). Potential of conventional & bispecific broadly neutralizing antibodies for prevention of HIV-1 subtype A, C & D infections. PLoS Pathog. 14, e1006860.

Wagih, O. (2017). ggseqlogo: a versatile R package for drawing sequence logos. Bioinformatics 33, 3645–3647.

Walker, L.M., Phogat, S.K., Chan-Hui, P.-Y., Wagner, D., Phung, P., Goss, J.L., Wrin, T., Simek, M.D., Fling, S., Mitcham, J.L., et al.; Protocol G Principal Investigators (2009). Broad and potent neutralizing antibodies from an African donor reveal a new HIV-1 vaccine target. Science 326, 285–289.

Walker, L.M., Huber, M., Doores, K.J., Falkowska, E., Pejchal, R., Julien, J.-P., Wang, S.-K., Ramos, A., Chan-Hui, P.-Y., Moyle, M., et al.; Protocol G Principal Investigators (2011). Broad neutralization coverage of HIV by multiple highly potent antibodies. Nature 477, 466–470.

Wang, H., Gristick, H.B., Scharf, L., West, A.P., Galimidi, R.P., Seaman, M.S., Freund, N.T., Nussenzweig, M.C., and Bjorkman, P.J. (2017). Asymmetric recognition of HIV-1 Envelope trimer by V1V2 loop-targeting antibodies. eLife 6, 1–25.

Ward, A.B., and Wilson, I.A. (2017). The HIV-1 envelope glycoprotein structure: nailing down a moving target. Immunol. Rev. 275, 21–32.

Wibmer, C.K., Bhiman, J.N., Gray, E.S., Tumba, N., Abdool Karim, S.S., Williamson, C., Morris, L., and Moore, P.L. (2013). Viral escape from HIV-1 neutralizing antibodies drives increased plasma neutralization breadth through sequential recognition of multiple epitopes and immunotypes. PLoS Pathog. 9, e1003738.

Wu, X., Parast, A.B., Richardson, B.A., Nduati, R., John-Stewart, G., Mbori-Ngacha, D., Rainwater, S.M.J., and Overbaugh, J. (2006). Neutralization Escape Variants of Human Immunodeficiency Virus Type 1 Are Transmitted from Mother to Infant. J. Virol. 80, 835–844.

Wu, X., Yang, Z.-Y., Li, Y., Hogerkorp, C.-M., Schief, W.R., Seaman, M.S., Zhou, T., Schmidt, S.D., Wu, L., Xu, L., et al. (2010). Rational design of envelope identifies broadly neutralizing human monoclonal antibodies to HIV-1. Science 329, 856–861.

Wu, N.C., Xie, J., Zheng, T., Nycholat, C.M., Grande, G., Paulson, J.C., Lerner, R.A., and Wilson, I.A. (2017). Diversity of Functionally Permissive Sequences in the Receptor-Binding Site of Influenza Hemagglutinin. Cell Host Microbe 22, 247–248.

Yoon, H., Macke, J., West, A.P., Jr., Foley, B., Bjorkman, P.J., Korber, B., and Yusim, K. (2015). CATNAP: a tool to compile, analyze and tally neutralizing antibody panels. Nucleic Acids Res. 43 (W1), W213–W219.

Zanini, F., Puller, V., Brodin, J., Albert, J., and Neher, R.A. (2017). In vivo mutation rates and the landscape of fitness costs of HIV-1. Virus Evol. 3, vex003.

CellPress

STAR★METHODS

KEY RESOURCES TABLE

REAGENT or RESOURCE	SOURCE	IDENTIFIER
Antibodies		
PGT151	Falkowska et al., 2014	GenBank: KJ700290.1, KJ700282.1
N123-VRC34.01	Kong et al., 2016	N/A
VRC01	Wu et al., 2010	aidsreagents.org; Cat # 12033
3BNC117	Scheid et al., 2011	aidsreagents.org; Cat # 12474
10-1074	Mouquet et al., 2012	aidsreagents.org; Cat # 12477
PGT121	Walker et al., 2011	aidsreagents.org; Cat # 12343
10E8	Huang et al., 2012	aidsreagents.org; Cat # 12294
PGT145	Walker et al., 2011	aidsreagents.org; Cat # 12703
PG9	Walker et al., 2009	aidsreagents.org; Cat # 12149
Bacterial and Virus Strains		
BG505.W6M.C2.T332N *env*	Wu et al., 2006	GenBank: DQ208458
Q23	Poss and Overbaugh, 1999	N/A
Q23.BG505.T332N	Haddox et al. 2018	aidsreagents.org; Cat # 8129
Deposited Data		
Illumina deep sequencing data	NCBI Sequence Reads Archive	SRR: 7693968–SRR: 7694021, SRR: 7758666, SRR: 8168127-SRR: 8168140
Experimental Models: Cell Lines		
SupT1.CCR5	James Hoxie	N/A
TZM-bl	NIH AIDS Reagents; contributed by Dr. John C. Kappes, Dr. Xiaoyun Wu and Tranzyme Inc.	aidsreagents.org; Cat # 8129
Oligonucleotides		
BG505 barcoded subamplicon deep sequencing primers	Haddox et al. 2018	N/A
Recombinant DNA		
Q23.BsmBI.BG505.T332N	Haddox et al. 2018, available at aidsreagents.org	aidsreagents.org; Cat # 13346
BG505.T332N mutant proviral libraries (n = 3)	Haddox et al. 2018, available at aidsreagents.org	aidsreagents.org; Cat # 13346
Software and Algorithms		
dms_tools2	Bloom, 2015	https://jbloomlab.github.io/dms_tools2/index.html
Mutational antigenic profiling pipeline	This paper	https://github.com/jbloomlab/EnvsAntigenicAtlas/

CONTACT FOR REAGENT AND RESOURCE SHARING

Further information and requests for resources and reagents should be directed to and will be fulfilled by the Lead Contact, Jesse Bloom (jbloom@fredhutch.org).

EXPERIMENTAL MODEL AND SUBJECT DETAILS

SupT1.CCR5 cells (Dr. James Hoxie) are SupT1 cells lentiviral transduced to express CCR5. SupT1 cells are a T cell lymphoblast originally isolated from 8-year-old Caucasian male with T cell lymphoblastic lymphoma. Cells were maintained as previously described (Haddox et al., 2018) at 37°C in the presence of 5% CO_2. These cells were verified to be mycoplasma free and closely related to the parental SupT1 cell line using STR profiling.

METHOD DETAILS

Generation of Mutant Virus Libraries

We have previously described the BG505.T332N mutant proviral DNA libraries and the resulting functional mutant virus libraries (Haddox et al., 2018). In brief, triplicate mutant BG505.W6M.C2.T332N *env* libraries that contained randomized codon-level mutations to sites 31-702 (HXB2 numbering is used here and throughout this manuscript) were independently generated and cloned into Q23.BsmBI.ΔEnv proviral plasmid (Haddox et al., 2018). These proviral plasmid libraries, as well as wild-type proviral plasmid, were transfected into 293T cells (obtained from ATCC). We then passaged the transfection supernatant at an MOI of 0.01 TZM-bl infectious units/cell in SupT1.CCR5 cells. The resulting genotype-phenotype linked mutant virus libraries were concentrated via ultracentrifugation.

Mutational Antigenic Profiling

The Env mutational antigenic profiling approach has been previously described (Dingens et al., 2017, 2018). Briefly, 0.5 - 1×10^6 TZM-bl infectious units of independent mutant virus libraries were neutralized with each antibody at an $\sim IC_{95}$ - $IC_{99.9}$ concentration for one hour. Libraries were then infected into 1×10^6 SupT1.CCR5 cells in R10 (RPMI, supplemented with 10% FBS, 1% 200 mM L-glutamine, and 1% of a solution of 10,000 units/mL penicillin and 10,000 μg/mL streptomycin) containing 100ug/mL DEAE-dextran. In parallel to each antibody selection, each mutant virus library was also infected into 1×10^6 SupT1.CCR5 cells without antibody selection to serve as the experiment-specific non-selected control. Four 10-fold serial dilutions of each mutant virus library were also infected into 1×10^6 cells as an infectivity standard curve. Cells were resuspended in 1 mL fresh R10 at three hours post infection. Cells were washed with PBS, pelleted, and non-integrated viral DNA was isolated via a miniprep at twelve hours post infection. The amount of viral genome in each sample was quantified via qPCR (Benki et al., 2006) or ddPCR (Dingens et al., 2017), and the fraction of each selected library that survived antibody selection relative to the non-selected control was interpolated from the infectivity standard curve.

Barcoded Subamplicon Deep Sequencing

The *env* gene was then amplified and sequenced using a barcoded subamplicon sequencing approach as previously described (Haddox et al., 2018) and explained in more detail at https://jbloomlab.github.io/dms_tools2/bcsubamp.html. Briefly, we first amplified the entire *env* gene from the harvested non-integrated viral DNA. This full-length *env* amplicon was then used as a template for amplifying 7 subamplicons that tile across *env*. Each of these subamplicons contained primer-introduced random barcodes on each end (8×N). Subamplicons are then bottlenecked such that the number of unique ssDNA molecules is less than the sequencing depth and then subjected to a final round of PCR that added the remainder of the Illumina sequencing adapters. All amplicons were then pooled and sequenced on Illumina HiSeq 2×250 bp runs. Errors introduced during sequencing were corrected by taking the consensus sequence at each site for each uniquely tagged ssDNA molecule as described in more detail in the Data S3.

Structural Analyses

Antibody contact sites were defined from Env-antibody structural models. The PDB models used were: 5FYK for VRC01 (Stewart-Jones et al., 2016), 5V8M for 3BNC117 (Lee et al., 2017), 5T3Z for 10-1074 (Gristick et al., 2016), 3U4E for PG9 (McLellan et al., 2011), 5V8L for PGT145 (Lee et al., 2017), 5FUU for PGT151 (Lee et al., 2016), 5I8H for VRC34.01 (Kong et al., 2016), 4G6F and for 10E8 (Huang et al., 2012). High resolution models of PGT121 bound to Env are not available; we used a model of PGT122 (PDB: 5FYL) (Stewart-Jones et al., 2016), which is a closely related "PGT121-like" clonal variant of PGT121 (Mouquet et al., 2012). Contact residues were defined as any Env residue where a non-hydrogen atom comes within 4 Å of any non-hydrogen antibody atom. When an antibody contacted a glycan, the N of that glycan's PNG was counted as a contact. For asymmetric antibody-trimer structures, the closest distance of the three antibody-Env residue distances was used.

For Figures 3, 4, and 5, we used the same structural models (with one exception) to generate figures using PyMol. While we used the high resolution PG9-V2 scaffold structure (McLellan et al., 2011) to determine contact sites, we mapped the fraction-surviving values onto the moderate resolution model of PG9 in complex with BG505 trimer (PDB: 5VJ6) (Wang et al., 2017) in Figure 3F to better illustrate the quaternary aspect of this apex epitope.

TZM-bl Neutralization Assays

TZM-bl neutralization assays using BG505.T332N pseudoviruses bearing single additional point mutants were performed. Briefly, serial dilutions of each antibody were incubated with 500 infectious units of pseudovirus for one hour before the addition of 10,000 TZM-bl reporter cells in the presence of 10 mg/mL DEAE-dextran. Forty-eight hours post-infection, infectivity was read by beta-galactosidase activity using Gal-Screen (Thermo Fisher Scientific, T1028). The assay was performed in duplicate two or three independent times, and fold change in IC_{50} of each mutant relative to BG505.T332N wild-type pseudovirus was calculated independently for each experiment and then averaged across all replicates.

QUANTIFICATION AND STATISTICAL ANALYSIS

Analysis of Deep Sequencing Data and Computation of Fraction Surviving

We used dms_tools2 version 2.2.9 (https://jbloomlab.github.io/dms_tools2/) to analyze the deep sequencing data and calculate the fraction surviving (Bloom, 2015). The calculation of the fraction surviving statistic has been described previously (Doud et al., 2018) and is documented in detail at https://jbloomlab.github.io/dms_tools2/fracsurvive.html. Sequencing of wild-type proviral DNA plasmid was used as the error control during the calculation of the fraction surviving. We took the median values across all experimental replicates for each antibody and plotted the excess fraction-surviving data on logoplots rendered by dms_tools2 using weblogo (Crooks et al., 2004) and ggseqlogo (Wagih, 2017).

Identification of Significant Sites of Viral Escape

Because the signal to noise ratio appeared to differ between antibodies, we defined statistically significant sites of viral escape beyond background individually for each antibody. For each antibody, we fit a gamma distribution to binned site fraction-surviving values (median values across all replicates) using robust regression (soft L1 loss as implemented in scipy). We then identified sites that fell outside the range of values expected from this distribution at a false discovery rate of 0.01 (Figure S2). For the purposes of Figures 2B and 2C, multiple sites that disrupted a PNG that the antibody contacted was considered a single site of escape. However, when the antibody also contacted the second or third protein residues in the PNG and that site was site of significant escape, the site treated as additional site of escape.

DATA AND SOFTWARE AVAILABILITY

Open-source software to analyze mutational antigenic profiling datasets is available at https://jbloomlab.github.io/dms_tools2/. The computational analysis is provided as an executable and HTML Jupyter notebook (Data S3) and at https://github.com/jbloomlab/EnvsAntigenicAtlas, and the fraction-surviving and excess fraction-surviving values for each antibody are provided as Data S4. Illumina deep sequencing reads are available from the NCBI SRA as study SRP157948, BioProject PRJNA486029, accession numbers SRR: 7693968-SRR: 7694021, SRR: 7758666, and SRR: 8168127-SRR: 8168140.

Supplemental Information

An Antigenic Atlas of HIV-1 Escape

from Broadly Neutralizing Antibodies

Distinguishes Functional and Structural Epitopes

Adam S. Dingens, Dana Arenz, Haidyn Weight, Julie Overbaugh, and Jesse D. Bloom

Supplemental Figures and Files

Data S1 | The excess fraction surviving values plotted across the length of the mutagenized portion of Env for each antibody. Related to Figures 2-5. The underlay indicates contact sites, sites of significant escape, and the overlap between these groups of sites, as in Figure 2B, 2C.

Data S2 | The excess fraction surviving PGT151 and VRC01 plotted across the mutagenized portion of different Envs. Related to Figures 2, S6, and S7.

Data S3 | The computational analysis. Related to Figure 2 and DATA AND SOFTWARE AVAILABILITY in the STAR Methods. A zip file containing an executable Jupyter notebook, an HTML version of the notebook, and all of the necessary input data to run the analysis.

Data S4 | The mutation fraction surviving and excess mutation fractions surviving datasets. Related to Figure 2. A zip file containing three CSV files for each antibody. One contains the mutation fraction surviving estimates, and one contains the excess mutation fraction surviving estimates plotted in the paper. The third contains *differential selection* estimates, which are log-transformed relative enrichment ratios that may be of use for certain purposes, such as examining mutations that are differentially depleted, rather than enriched, upon antibody selection. The differential selection metric is described in detail in (Doud et al., 2017) and at https://jbloomlab.github.io/dms_tools2/diffsel.html. Sites are numbered according to HXB2 reference strain numbering.

A.

antibody	antibody concentration per mL	library	fraction surviving	percent neutralized
VRC01	11ug	1	0.002029	99.80
	8ug	2	0.027775	97.22
	11ug	2	0.009827	99.02
	11ug	3	0.001008	99.90
	11ug	3	0.007226	99.28
3BNC117	4ug	1b	0.008765	99.12
	3ug	2b	0.009847	99.02
	4ug	3b	0.006475	99.35
	4ug	2b	0.022027	97.80
PGT121	4-25ug	2b	0.003383	99.66
	3-5ug	2b	0.007412	99.26
	3-5ug	3b	0.012455	98.75
	3-5ug	1	0.010645	98.94
10-1074	3ug	2b	0.019202	98.08
	4ug	2b	0.015257	98.47
	4ug	3b	0.003771	99.62
	4ug	1b	0.011481	98.85
PG9	10ug	1	0.025034	97.50
	10ug	3	0.016036	98.40
PGT145	125ug	2b	0.028826	97.12
	125ug	1b	0.031111	96.89
	125ug	3b	0.033075	96.69
PGT151	0.2ug	3	0.035396	96.46
	0.2ug	1	0.020718	97.93
VRC34	33ug	3	0.050239	94.98
	33ug	1	0.063644	93.64
10E8	60ug	1	0.001157	99.88
	60ug	3	0.002491	99.75

B.

C.

antibody	antibody concentration (each) per mL	replicate	fraction surviving	percent neutralized
3BNC117 and 10-1074 pooled	3ug	1b	0.00142	99.858
	3ug	3b	0.001521	99.8479
	4ug	1b	0.001074	99.8926
	4ug	3b	0.000413	99.9587
	4ug	2b	0.000341	99.9659
	3ug	2b	0.001887	99.8113

D.

E.

virus	antibody	antibody concentration per mL	library	fraction surviving	percent neutralized
LAI	PGT151	2ug	1	0.039071	96.09
		2ug	2	0.021078	97.89
		2ug	3	0.014522	98.55
BF520	PGT151	1ug	1	0.0185	98.15
		1ug	2	0.0239	97.61
		1ug	3	0.0495	95.05
BG505	PGT151	0.2ug	3	0.035396	96.46
		0.2ug	1	0.020718	97.93
BG505	VRC01	11ug	1	0.002029	99.80
		8ug	2	0.027775	97.22
		11ug	2	0.009827	99.02
		11ug	3	0.001008	99.90
		11ug	3	0.007226	99.28
LAI	VRC01	9ug	3	0.067211	93.28
		11ug	3	0.061111	93.89
		14ug	1	0.090284	90.97
		14ug	2	0.033175	96.68
		14ug	3	0.021007	97.90

F.

G.

H.

Figure S1 | The fraction surviving measurements and correlation between mutational antigenic profiling biological replicates. Related to Figure 2, 6, S6, and S7. A. For each biological replicate, the antibody concentration used during the selection, which mutant virus library was used, and the fraction of that library that survived antibody selection is shown. For clarity, the percent neutralized (1- library

fraction surviving) × 100 is also shown. **B.** The correlation between the average excess

fraction surviving at each site for each biological replicate, for each antibody. **C.** As in A,

but for biological replicates of pooled 3BNC117 and 10-1074. **D.** As in B, but for pooled

3BNC117 and 10-1074. **E.** As in A, but for biological replicates for PGT151 and

VRC01 using LAI and BF520 mutant Env libraries. **F.** As in B, but for PGT151

escape using LAI mutant Env libraries. **G.** Same as F, but for BF520 mutant Env

libraries. **H.** The same as F, but for escape from VRC01 using LAI mutant virus

libraries.
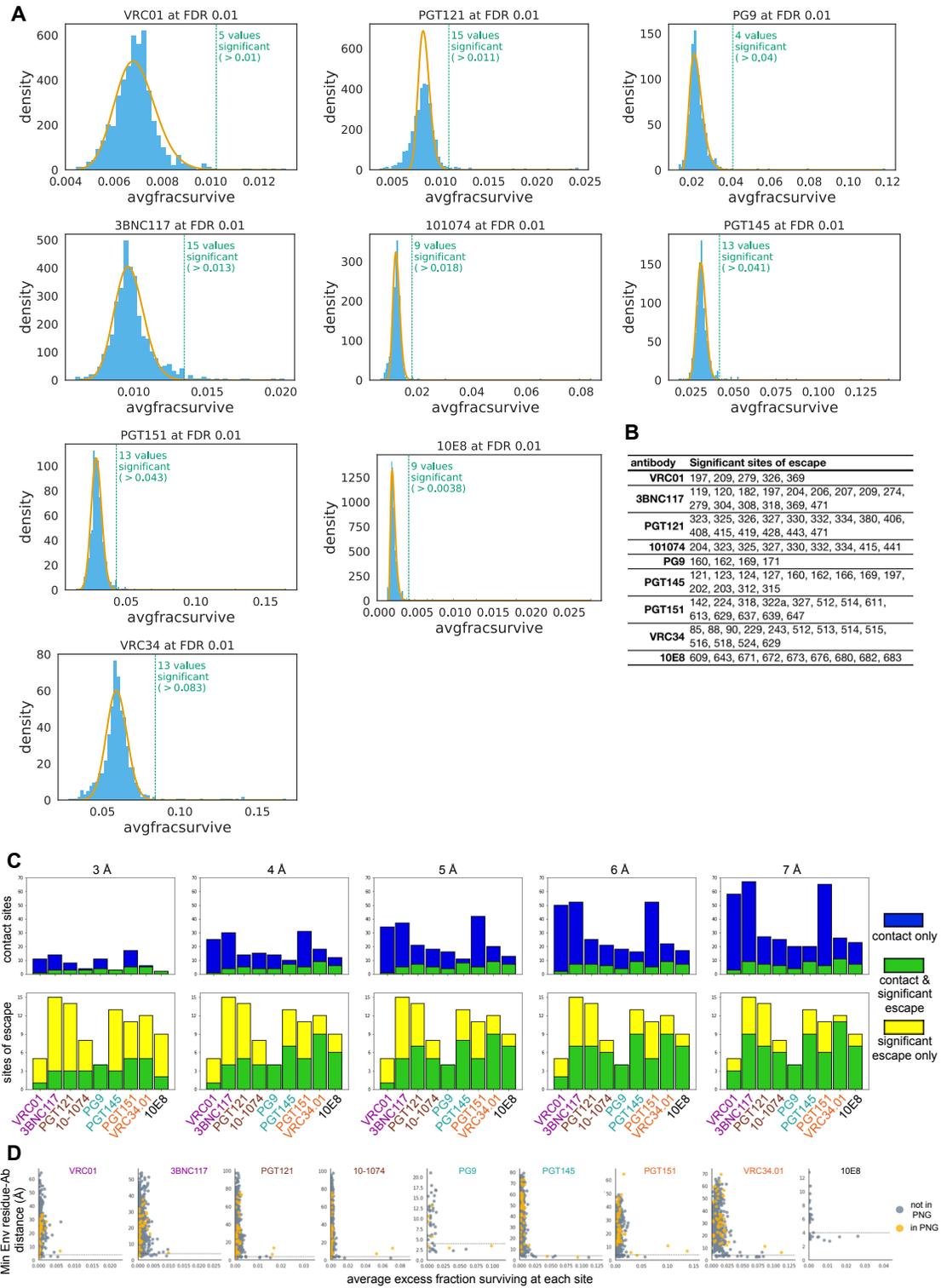
Figure S2 | Identification of significant sites of viral escape and the overlap between each antibody's structural and functional epitope. Related to Figure 2. A.

For each antibody, the distribution of the average fraction surviving at each site is plotted in blue. A gamma distribution fit to the site fraction surviving values using robust regression is overlaid in yellow. A dotted line shows sites that fall beyond this distribution at a fall discovery rate of 0.01, and the number of sites that beyond this cutoff is labeled. Code that performs this analysis is at

https://jbloomlab.github.io/dms_tools2/dms_tools2.plot.html#dms_tools2.plot.findSigSel.

B. A table listing all of the significant sites of viral escape for each antibody.

C. As in Figure 2B and 2C, but using different distance cutoffs between non-hydrogen Env and antibody atoms to determine contact sites**. D.** For each Env residue in our library the minimum distance to the antibody is plotted against that site's excess fraction surviving averaged across mutations. The 4 Å distance cutoff used in Figure 2B and 2C is plotted with a dotted line. Sites that fall within PNGs are colored yellow, while other sites are grey. Only sites that are in the structures used to determine distance cutoffs are plotted (see STAR Methods for details of the structures used).

A

10-1074

Mutation	Mutation fraction surviving	Fold Change IC$_{50}$ relative to WT	Mutational effect on viral growth
C119R	0.008278	0.8	0.097958
D140E	0.008363	1.6	1.533243
R151K	0.011343	1.6	0.767443
D322A	0.009009	0.8	1.117847
D322E	0.008749	1.4	0.834735
D322G	0.006662	1.4	0.889122
I323G	0.035657	2.5	1.472166
D325E	0.063118	27.2	1.383803
D325N	0.010407	0.7	1.410747
D325S	0.044115	3.0	2.545381
I326Y	0.009754	0.9	0.42606
R327A	0.035596	4.0	0.527711
H330R	0.048421	35.1	0.114338
T415R	0.068193	4.8	1.050657
T415Y	0.041935	2.7	1.76969
G441P	0.014016	2.2	0.24461

PGT121

Mutation	Mutation fraction surviving	Fold Change IC$_{50}$ relative to WT	Mutational effect on viral growth
C119R	0.01423	1.2	0.097958
D140E	0.002981	1.6	1.533243
R151K	0.008765	1.3	0.767443
D322A	0.018474	1.1	1.117847
D322E	0.004105	1.4	0.834735
D322G	0.009586	1.4	0.889122
I323G	0.032053	1.9	1.472166
D325E	0.009864	1.7	1.383803
D325N	0.003128	0.8	1.410747
D325S	0.007069	1.2	2.545381
I326Y	0.008386	1.3	0.42606
R327A	0.037228	3.4	0.527711
H330R	0.017344	1.6	0.114338
T415R	0.073432	3.8	1.050657
T415Y	0.034631	2.4	1.76969
G441P	0.008918	2.6	0.24461

VRC01

Mutation	Mutation fraction surviving	Fold Change IC$_{50}$ relative to WT	Mutational effect on viral growth
D113N	0.014156	4.1	0.040187
C119R	0.011311	1.6	0.097958
D140E	0.008087	1.8	1.533243
R151K	0.015409	1.7	0.767443
N197E	0.005161	0.02	0.272265
N197S	0.058665	26.1	0.380752
T198A	0.039597	3.6	0.15237
N279K	0.035774	>175	0.006956
I323G	0.005812	1.1	1.472166
D325E	0.002185	0.8	1.383803
D325N	0.002956	0.8	1.410747
D325S	0.005692	0.9	2.545381
I326Y	0.042948	2.9	0.42606
R327A	0.010742	1.3	0.527711
H330R	0.009456	0.9	0.114338
L369K	0.031735	4.01	0.888277
T415R	0.007226	0.9	1.050657
T415Y	0.00695	0.9	1.76969
G441P	0.011296	1.4	0.24461

PGT145 Data from Lee *et al. Immunity* 2017

Mutation	Mutation fraction surviving	Fold Change IC50 relative to WT	Mutational effect on viral growth
K121A	0.069501	302	0.18497
V127A	0.049786	302	0.065149
N156K	0.075847	302	0.029769
N160A	0.061076	302	0.175816
N160K	0.091395	302	0.410596
M161A	0.022357	60.4	1.083304
T162A	0.112894	302	0.112595
E164A	0.041677	2.7	0.056266
L165A	0.031111	167.1	0.006771
R166A	0.196633	302	1.510136
D167A	0.031111	302	0.01187
K168A	0.025926	274.8	0.091057
K169A	0.046097	256.2	0.80713
I307A	0.028948	0.3	0.005547
I420A	0.020672	3.8	0.949832
I423A	0.033075	1.9	0.014982

B

Figure S3 | Mutational antigenic profiling results are validated by TZM-bl neutralization assays. Related to Figure 2. A. The tables list mutations that were selected for validation in neutralization assays. Data for PGT145 was taken from (Lee et al., 2017). For each mutation, the table gives the mutation's fraction surviving antibody, fold change in IC$_{50}$ in the TZM-bl neutralization assay, and the mutation's effect on viral growth. The mutation's effect on viral growth is calculated from our prior deep mutational scanning of Env for viral growth in cell culture, in the absence of any immune selection (Haddox et al., 2018). The mutational effect is the ratio of the preference for that mutant amino acid relative to the wildtype amino acid at that site. If the mutational effect is >1, then that mutation grows better than wildtype in cell culture; if it is <1, that mutant grows worse than wildtype. **B.** For each antibody, we plot the correlation between the mutation fraction surviving and the fold change in IC$_{50}$ relative to wildtype from TZM-bl assays. Points are colored according the log$_2$ mutational effect of the mutation on viral growth (note these are the log$_2$ transformed values displayed in A). Where there are discrepancies between mutational antigenic profiling and TZM-bl assays, these mutants (e.g. N279K for VRC01; H330R for 10-1074) often have log$_2$ mutational effects on viral growth <<0 (darker blue), indicating they are deleterious for viral growth in cell culture.

Heavy chain:
| FWR1 | CDR1 | FWR2 | CDR2 | FWR3 | CDR3 | FWR4 |

```
                    10        20        30        40        50        60        70        80        90       100       110
GL       QVQLQESGPGLVKPSETLSLTCTVSGGSISSYYWSWIRQPPGKGLEWIGYIYYSGSTNYNPSLKSRVTISVDTSKNQFSLKLSSVTAADTAVYYCARTQQGKRIYGVVSFGDYYYYYYMDVWGKGTTVTVSS

PGT121   QMQLQESGPGLVKPSETLSLTCSVSGASISDSYWSWIRRSPGKGLEWIGYVHKSGDTNYSPSLKSRVNLSLDTSKNQVSLSLVAATAADSGKYYCARTLHGRRIYGIVAFNEWFTYFYMDVWGNGTQVTVSS
10-1074  QVQLQESGPGLVKPSETLSVTCSVSGDSMNNYYWTWIRQSPGKGLEWIGYISDRESATYNPSLNSRVVISRDTSKNQLSLKLNSVTPADTAVYYCATARRGQRIYGVVSFGEFFYYYSMDVWGKGTTVTVSS
```

Light chain:
| FWR1 | CDR1 | FWR2 | CDR2 | FWR3 | CDR3 | FWR4 | Variable region annotation: **Kabat** **IMGT** |

```
                  12      20        30        40        50        60        70        80        90       100
GL       SYVLTQPPSVSVAPGQTARITCGGNNIGSKSVHWYQQKPGQAPVLVVYDDSDRPSGIPERFSGS-NS--GNTATLTISRVEAGDEADYYCQVWDSSSDHPWVFGGGTKLTVL

PGT121   SDI-------SVAPGETARISCGEKSLGSRAVQWYQHRAGQAPSLIIYNNQDRPSGIPERFSGSPDSPFGTTATLTITSVEAGDEADYYCHIWDSRVPTKWVFGGGTTLTVL
10-1074  SYVRP----LSVALGETARISCGRQALGSRAVQWYQHRPGQAPILLIYNNQDRPSGIPERFSGTPDINFGTRATLTISGVEAGDEADYYCHMWDSRSGFSWSFGGATRLTVL
```

contacts N332 glycan
contacts site 325

Figure S4 | Sequence alignment of PGT121 and 10-1074 antibody chains. Related to Figure 3. The heavy (top) and light chain (bottom) genes of the clonal variants PGT121 and 10-1074 are aligned, along with their inferred germline (GL). Kabat and IMGT variable regions annotations are shown. There are several sites in Env where the effects of mutations differ markedly between PGT121 and 10-1074, most prominently sites 325 and the N332 PNG. We used the 10-1074 / Env co-crystal structure 5TZ3 to identify sites in 10-1074 that contact these Env sites, and have highlighted them in the alignment above PGT121 contact sites are not labeled, as there is not a high-resolution structure of available. The germline inference, alignment, and variable loop annotation are from Mouquet *et al.* 2012, which also discusses additional structural differences between these antibodies (such as differences in the light chain loops of the unliganded antibody structures).

Antibody	Study	ClinicalTrials.gov Identifier (NCT Number)	Study description	Overlap between **reported** sites of viral evolution during bnAb immunotherapy* and significant sites of viral escape from our mutational antigenic profiling
10-1074	Casket et al 2017	NCT02511990	Single infusion of 10-1074 to HIV infected individuals	**325**, **332**, **334**[A]
3BNC117	Caskey et al 2015, Schoofs et al 2016	NCT02018510	Single infusion of 3BNC117 to HIV infected individuals	**209**, **279**, **308**, **318**, **471**[B]
3BNC117	Scheid et al 2016	NCT02446847	Multiple (2-4) infusions of 3BNC117 after the discontinuation of antiretroviral therapy	**274**[C]
VRC01	Lynch et al 2015a	NCT01950325	One or two infusions of VRC01 in antiretroviral treated and untreated HIV-infected patients, respectively	none[D]
VRC01	Bar et al 2016	NCT02463227 and NCT02471326	Multiple (3-8) infusions of VRC01 after the discontinuation of antiretroviral therapy	**279**[E]; reanalysis of these data revealed potential selection at **326****

* The sites in this table were determined in each study individually, using disparate methods, explained below.

A: Discussed in main figures and text.

B: Used LASSIE (Longitudinal Antigenic Sequences and Sites from Intrahost Evolution) to identify sites selected within the 24-week time frame, using a selection cutoff changing ≥ 80% amino acid frequency compared to baseline. Indels are omitted from this group.

C: Discussed in text based on sequence alignments.

D: Used a neutralization-based epitope prediction (NEP) algorithm to predict mutational differences that could be associated with VRC01 selection. The top 5 highest scoring sites for the four patients examined are reported here.

E: Two separate criteria were used by the two clinical trials reported in Bar et al 2016. In one, the VRC01 antibody footprint sequence was analyzed using LASSIE, and we then identified sites within the examined regions that differed ≥50% amino acid frequency compared to baseline. In the other study, HIV env sequences were analyzed using a neutralization-based epitope prediction (NEP) algorithm. Changes in amino-acid residues that occurred within or next to the VRC01 epitope were reported.

**Examination of *env* genotype from this study in the context of our VRC01 escape profile revealed a potential additional site of viral escape not discussed in Bar *et al*. 2016. In Patient V10, T326 was fixed shortly after VRC01 treatment, but T326 was present in only 2/49 sequences at later timepoints when antibody levels may have waned (I326, present in the remaining sequences, is 96.8% conserved in the LANL filtered web alignment) (Bar et al., 2016). No pretreatment sequences were available.

Table S1 | Overlap between mutational antigenic profiling sites of escape and sites of viral evolution that occurred *in vivo* during bnAb immunotherapy. Related to Figures 3 and 4.
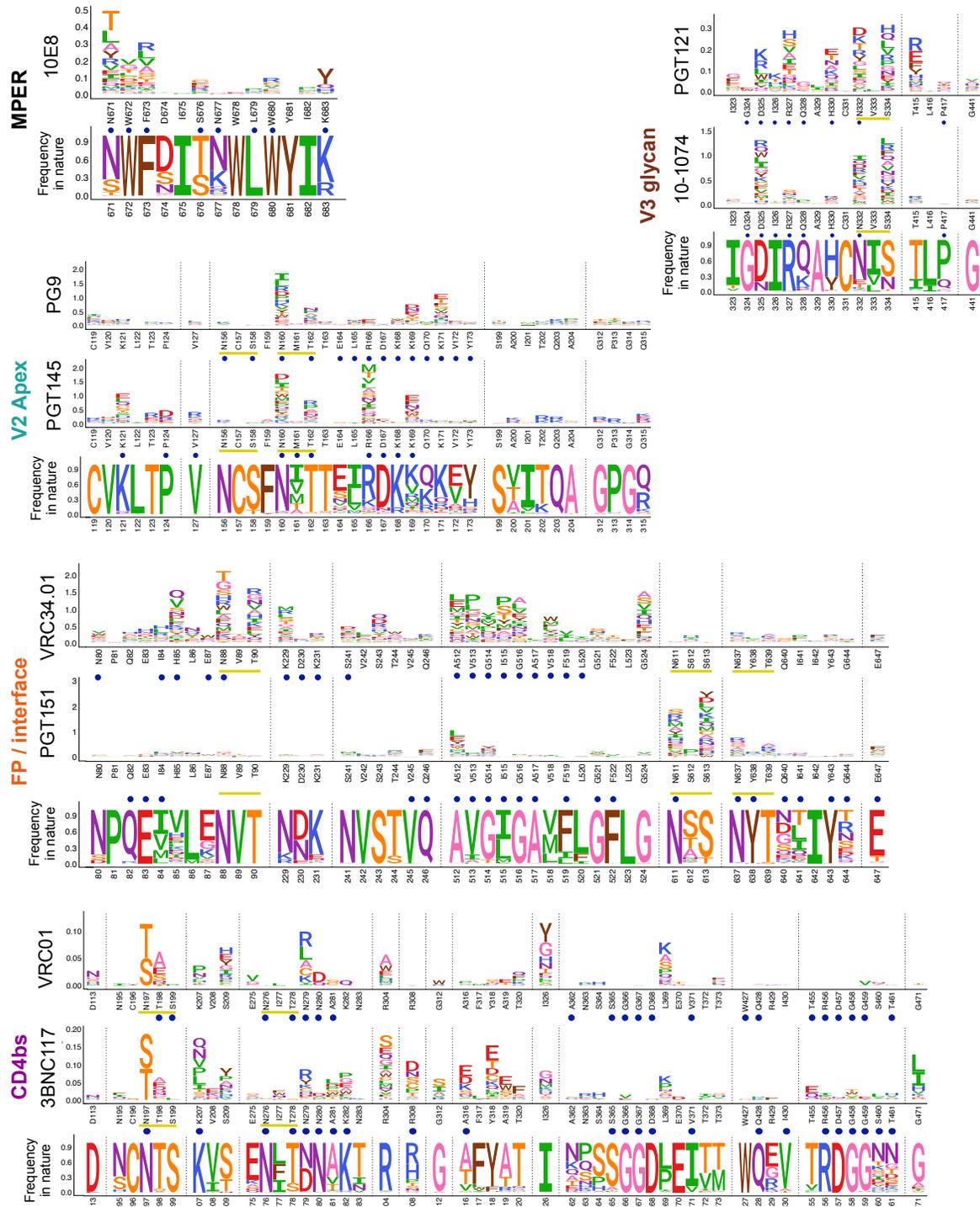
Figure S5 | The natural sequence variation of escape mutations. Related to Figure 7. For each epitope, the excess fraction surviving is shown for each

antibody, as in Figures 3-5. Blue circles indicate antibody structural contacts and yellow underlines indicate glycosylation motifs. On bottom, the frequency of amino acids in nature is also plotted. Natural sequence variation is based on LANL's group M filtered Web Alignment (Foley et al., 2017).
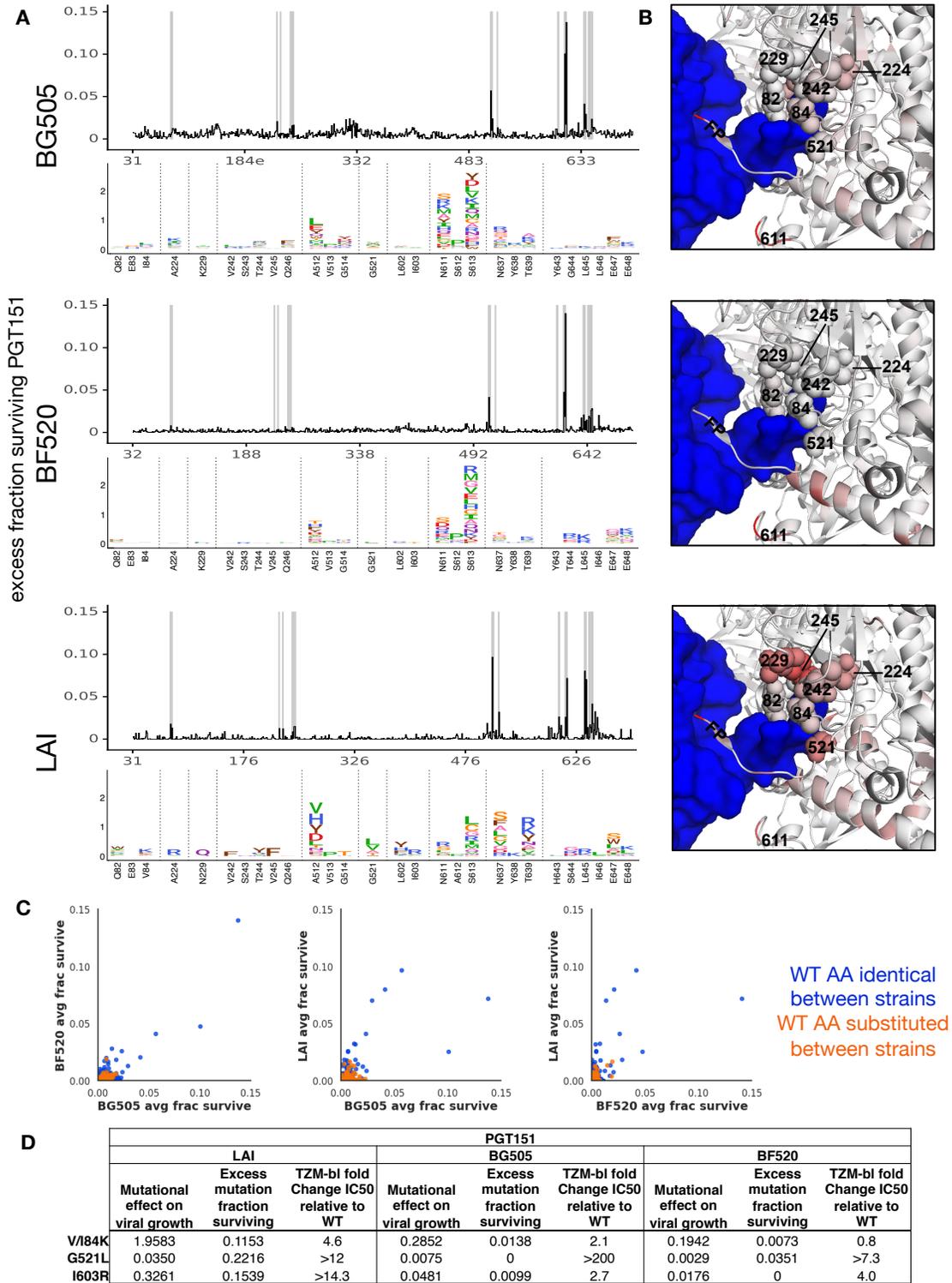
Figure S6 | Differences in PGT151 escape across Envs. Related to Figure 2.

A. The line plots shows each site's average excess fraction surviving PGT151 for

BG505, BF520, and LAI Env. Beneath, logoplots show the mutation level escape

profile for sites highlighted in grey in the line plots. The entire mutation-level

escape profile for each Env is available in File S2. **B.** View of the PGT151

epitope colored according to escape in each Env. PGT151 Fab is colored blue,

and Env is colored according to the maximum mutation fraction surviving at each

site for each strain (PDB:5FUU). **C.** The correlation between BG505, BF520, and

LAI excess fraction surviving PGT151 for each site. Sites are colored blue if the

wildtype amino acid is identical between strains, orange if they differ. **D.** The

mutational effect, excess mutation fraction surviving, and fold change in PGT151

IC_{50} from TZM-bl assays using point mutant pseudoviruses of validated point

mutants. As in Figure S4, the mutational effect is measured via deep mutational

scanning of each Env under selection for viral replication in cell culture in the

absence of any immune selection (Haddox et al 2016, Haddox et al 2018). The

mutational effect is the ratio of the preference of that mutant relative to the

wildtype amino acid preference at that site. If the mutational effect is >1, then that

mutation replicates better than wildtype in cell culture; if it is <1, that mutant

replicates worse than wildtype. Where there are discrepancies between

mutational antigenic profiling and TZM-bl assays, that mutation has an effect

<<1, indicating it is deleterious for viral replication in cell culture.

A ... **B**

C ... **D**

	VRC01					
	LAI			BG505		
	Mutational effect on viral growth	Excess mutation fraction surviving	TZM-bl fold Change IC50 relative to WT	Mutational effect on viral growth	Excess mutation fraction surviving	TZM-bl fold Change IC50 relative to WT
D113N	1.0627	0	0.6	0.0402	0.0121	4.1
M/I326Y	1.1315	0	0.7	0.4261	0.0355	2.9
P/L369K	3.2512	0.0119	1.5	0.8883	0.0219	4.0
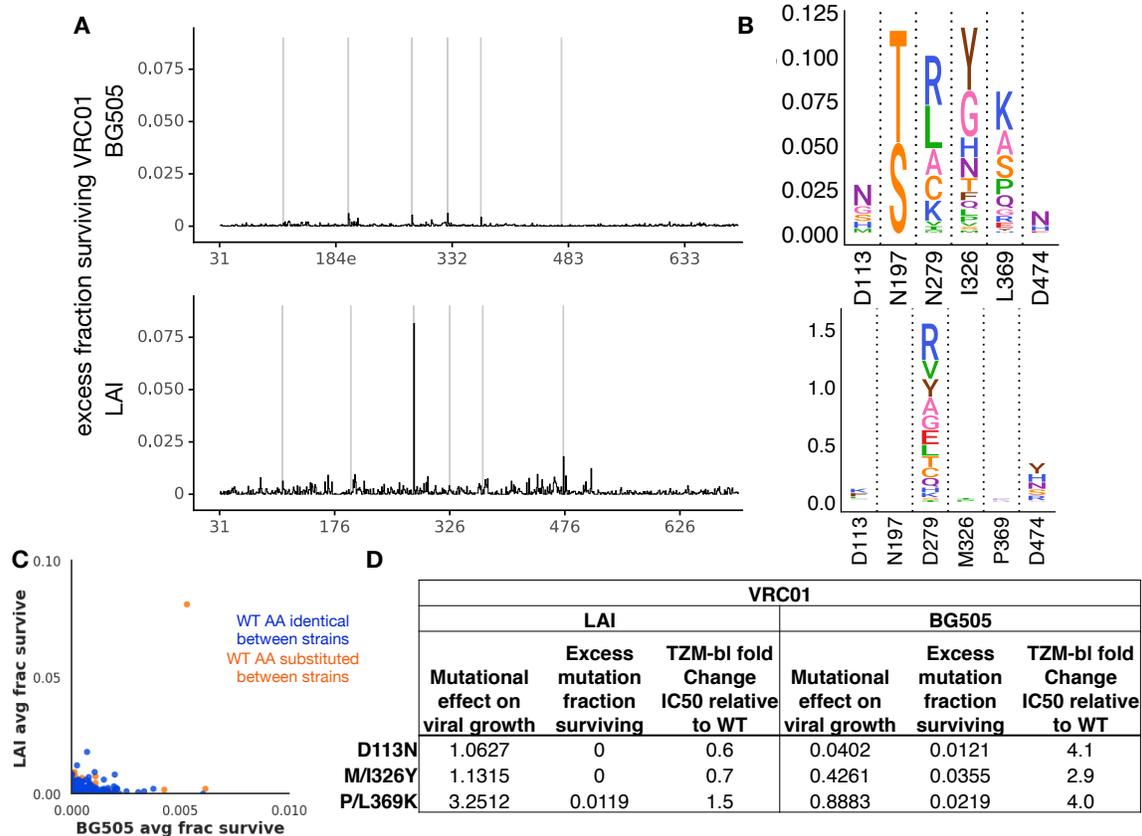
Figure S7 | Differences in VRC01 escape across Envs. Related to Figure 2.

A. The line plots shows each site's average excess fraction surviving VRC01 for BG505 and LAI Env. **B.** Logoplots show the mutation level escape profile for sites highlighted in grey in A. The entire mutation-level escape profile for both Envs is available in File S2. **C.** Same as in S6C, but for VRC01 escape in BG505 and LAI. **D.** Same as in S6D, but for validated VRC01 escape mutants.